Drosophila epidermal cells are intrinsically mechanosensitive and drive nociceptive behavioral outputs

Jiro Yoshino[1,2,3*], Sonali S. Mali[3,4,5*], Claire R. Williams[1,3*], Takeshi Morita[3,6], Chloe E. Emerson[3], Christopher J. Arp[3], Sophie E. Miller[3], Chang Yin[1], Lydia Thé[4], Chikayo Hemmi[2], Mana Motoyoshi[2], Kenichi Ishii[2], Kazuo Emoto[2,7#], Diana M. Bautista[3,4,5#], and Jay Z. Parrish[1,3#]

[1]Department of Biology, University of Washington, Campus Box 351800, Seattle, WA 98195, USA

[2]Department of Biological Sciences, Graduate School of Science, The University of Tokyo, 7-3-1 Hongo, Bunkyo-ku, Tokyo 113-0033 Japan

[3]Division of Education, Marine Biological Laboratory, 7 MBL Street, Woods Hole, MA 02543, USA

[4]Department of Molecular and Cell Biology, University of California, Berkeley, CA 94720, USA

[5]Helen Wills Neuroscience Institute, University of California, Berkeley, CA 94720, USA

[6]Laboratory of Neurogenetics and Behavior, The Rockefeller University, 1230 York Avenue, New York, NY 10065

[7]International Research Center for Neurointelligence (WPI-IRCN), The University of Tokyo, 7-3-1 Hongo, Bunkyo-ku, Tokyo 113-0033 Japan

*These authors contributed equally to this work

[#]Correspondence: jzp2@uw.edu (lead contact), dbautista@berkeley.edu, or emoto@bs.s.u-tokyo.ac.jp

Abstract

Somatosensory neurons (SSNs) that detect and transduce mechanical, thermal, and chemical stimuli densely innervate an animal's skin. However, despite the fact that epidermal cells provide the first point of contact for sensory stimuli. our understanding of roles that epidermal cells play in SSN function, particularly nociception, remains limited. Here, we show that stimulating *Drosophila* epidermal cells elicits activation of SSNs including nociceptors and triggers a variety of behavior outputs, including avoidance and escape. Further, we find that epidermal cells are intrinsically mechanosensitive and that epidermal mechanically evoked calcium responses require the store-operated calcium channel Orai. Epidermal cell stimulation augments larval responses to acute nociceptive stimuli and promotes prolonged hypersensitivity to subsequent mechanical stimuli. Hence, epidermal cells are key determinants of nociceptive sensitivity and sensitization, acting as primary sensors of noxious stimuli that tune nociceptor output and drive protective behaviors.

42 **Introduction**

The ability to detect tissue-damaging noxious stimuli and mount an escape
44 response is essential for survival. Likewise, prolonged hypersensitivity following injury is an important form of plasticity that protects an animal from further damage. In
46 *Drosophila*, a single class of identified somatosensory neurons (SSNs), class IV dendrite arborization (C4da) neurons, are necessary and sufficient for nociception;
48 inactivating C4da neurons renders larvae insensitive to noxious stimuli whereas activating these neurons drives nocifensive behavior responses (Hwang *et al.*, 2007; Hu
50 *et al.*, 2017; Burgos *et al.*, 2018). A variety of agents that cause tissue damage including UV irradiation and chemical toxins induce long-lasting allodynia and hyperalgesia
52 (Babcock *et al.*, 2009; Boiko *et al.*, 2017), but this damage-induced hypersensitivity develops on a timescale of hours. *Drosophila* also display acute hypersensitivity to
54 multiple noxious mechanical stimuli (Hu *et al.*, 2017). However, the cellular and molecular mechanisms underlying mechanical pain hypersensitivity remain enigmatic.

56 Recent studies demonstrate that epidermal cells work in concert with SSNs to transduce noxious and innocuous physical stimuli. For example, epidermal Merkel cells
58 are mechanosensory cells that signal to sensory neurons to mediate touch transduction (Maksimovic *et al.*, 2014; Hoffman *et al.*, 2018). Similarly, keratinocytes are directly
60 activated by noxious thermal and mechanical stimuli and release molecules that modulate nociceptor functions (Chung *et al.*, 2004; Koizumi *et al.*, 2004; Moqrich *et al.*,
62 2005; Mandadi *et al.*, 2009; Liu *et al.*, 2019; Sadler *et al.*, 2020). Furthermore, epidermal cells in invertebrates and vertebrates ensheath nociceptors in mesaxon-like structures
64 (Cauna, 1973; Chalfie and Sulston, 1981; Han *et al.*, 2012; Kim *et al.*, 2012a; O'Brien *et al.*, 2012), and these sheaths may serve as sites of epidermis-nociceptor signaling (Yin
66 *et al.*, 2021). Indeed, epidermal ensheathment is required for normal responses to noxious mechanical stimuli in *Drosophila* (Jiang *et al.*, 2019). However, whether
68 epidermal cells are directly activated by noxious stimuli and modulate C4da neuronal activity has not been studied.

70 Here, we examined the capacity of *Drosophila* epidermal cells to drive nociceptor activation and modulate mechanical nociceptive responses. We found that stimulation

of epidermal cells, but no other non-neuronal cell types in the larval body wall, is sufficient to activate a variety of SSNs neurons and trigger nocifensive behavioral responses. Our *in vitro* and *ex vivo* calcium imaging experiments demonstrate that epidermal cells are intrinsically mechanosensitive. Using an unbiased genetic screen, we discovered a role for the store-operated calcium channel Orai, and its activator Stim in epidermal mechanotransduction and mechanical sensitization. Downstream of Stim/Orai activation, epidermal cells drive nociceptor activation and mechanical hypersensitivity via epidermal vesicular release. Overall, we demonstrate that *Drosophila* epidermis-neuron signaling mediates both the acute detection of noxious mechanical stimuli and a form of prolonged mechanical hypersensitivity.

Results

Stimulation of epidermal cells evokes nocifensive behavior

To identify peripheral non-neuronal cell types that contribute to nociception, we conducted an optogenetic screen for light-evoked nocifensive behavior. First, as a benchmark for comparison we used the light-activated cation channel CsChrimson (Klapoetke *et al.*, 2014) to optogenetically activate nociceptive C4da neurons. Consistent with prior reports (Hwang *et al.*, 2007; Hu *et al.*, 2017), C4da activation triggered nocifensive behaviors including c-bending and rolling in 100% of larvae (Fig. 1A, Fig. 1S1A, Movie S1). Next, we selectively expressed CsChrimson using GAL4 drivers in combination with *elav-GAL80* (to block neuronal GAL4 activity) to target the six principle non-neuronal cell types within the larval body wall: epidermis, trachea, muscle, hemocytes, oenocytes, and glia (Fig. 1S2, Table S1). We then monitored light-evoked behavioral outputs associated with stimulation of each cell type. We found that optogenetic stimulation of epidermal cells, like C4da neurons, elicited c-bending or rolling in 73% of larvae (Fig. 1A, 1S1B), suggesting that epidermal cells are sufficient to drive nocifensive behaviors. Stimulation of other body wall cell types elicited a variety of non-nociceptive behavior outputs: for example, muscle stimulation triggered hunching behavior followed by prolonged freezing, whereas glia stimulation reproducibly induced only hunching behavior (Fig. 1S1C-I) (Zimmermann *et al.*, 2009). Thus, epidermal cells

102 are the only non-neuronal body wall cell type that triggers robust nocifensive behavioral responses.

104 To further validate the selective ability of body wall epidermal cells to drive nocifensive behaviors, we examined eight other epidermal drivers in addition to 106 *R38F11-GAL4* (which displays limited non-epidermal cell expression in larvae; Fig. 1S3). We found that optogenetic stimulation evoked nocifensive behaviors in all eight 108 lines: seven of the lines displayed rolling behavior while all eight displayed c-bending (Fig. 1B, Fig. 1S4). The previously described pan-epidermal *A58-GAL4* driver (Galko 110 and Krasnow, 2004) drove robust nocifensive rolling responses (Fig. 1B, 1S4), although we note that *A58-GAL4* is expressed broadly in the larval CNS (Fig. 1S5). While the 112 remaining seven drivers displayed epidermal specificity, most of the lines labeled subsets of epidermal cells (Fig. 1S5), and the nocifensive behavioral response 114 correlated with the proportion of epidermal expression (Fig 1B).

We next used thermogenetic stimuluation with the warmth-activated TRP 116 channel dTRPA1 (Hamada *et al.*, 2008) as an independent method of probing epidermal cell-evoked nociception. We found that >75% of larvae expressing TRPA1 in 118 nociceptors exhibited heat-dependent rolling behavior (Fig. 1C). Likewise, larvae that expressed TRPA1 pan-epidermally (*R38F11-GAL4*) with or without *elav-GAL80* 120 exhibited robust rolling responses (Fig. 1C, Fig. 1S3). In contrast, the thermal stimulus (35° C) rarely induced rolling behavior in control larvae bearing *UAS-TRPA1* alone. 122 Altogether, these results demonstrate that epidermal stimulation evokes nocifensive responses in *Drosophila*.

124 In addition to C4da nociceptors, the epidermis is innervated by a variety of other SSNs including mechanosensory C3da and chordotonal (Cho) neurons. Whereas direct 126 stimulation of C4da nociceptors principally elicited nocifensive behavioral outputs, epidermal stimulation elicited an array of behaviors in addition to nocifensive responses, 128 including freezing and hunching (Fig. 2A, 2B), behaviors associated with stimulation of C3da and Cho neurons (Zhang *et al.*, 2013; Turner *et al.*, 2016). These data suggest 130 that epidermal cells may broadly modulate SSN activity in *Drosophila*.

To examine whether different epidermis-evoked behaviors were associated with
132 activation of distinct classes of SSNs, we compared epidermis-evoked and SSN-evoked behaviors. C4da, C3da and Cho stimulation elicited distinct behavioral motifs: only
134 C4da neurons elicited rolling behavior; C3da neurons elicited hunching, C-bending, and backing; Cho neurons principally elicited hunching and freezing responses (Fig. 2C-2E).
136 In contrast, optogenetic epidermal stimulation elicited all of these behaviors in a stereotyped sequence, with nocifensive behaviors (c-bending, rolling) preceding non-
138 nociceptive behaviors (backing, freezing) (Fig. 2B, 2S1).

We observed three striking differences in behavior evoked by stimulation of
140 epidermal cells versus individual SSNs. First, although rapid, latency to rolling was significantly longer following epidermal stimulation compared to stimulation of C4da
142 (Fig. 2F). Second, the duration of rolling, bending, and backing responses was significantly longer for epidermis versus SSN stimulation (Fig. 2G). Third, backing and
144 freezing behaviors persisted beyond the duration of the light stimulus for epidermis but not SSN stimulation (Fig. 2H). In summary, we find that epidermal stimulation triggers
146 more robust, varied and prolonged behaviors compared to responses from direct stimulation of discrete SSN subtypes.

148

Somatosensory neurons are activated by epidermal stimulation

150 We next asked whether epidermal stimulation activates C4da, C3da, and Cho neurons. To test this possibility, we developed a semi-intact larval preparation in which we
152 optogenetically stimulated epidermal cells while simultaneously monitoring calcium responses in axon terminals of SSNs (Fig. 3A). We found that epidermal stimulation
154 triggered rapid and robust calcium transients in nociceptive C4da, and mechanosensory C3da and Cho neurons (Fig. 3A-3D, 3S1).

156 We next tested the requirement for SSN synaptic transmission in epidermis-evoked behaviors. We stimulated epidermal cells with CsChrimson while blocking SSN
158 neurotransmitter release using tetanus toxin light chain (TnT) (Sweeney *et al.*, 1995). We found that inhibiting C4da or C3da neurotransmission significantly reduced the
160 frequency and duration of epidermal-evoked rolling and backing behaviors, respectively

(Fig. 3E, 3F, 3S2). These data suggest that C4da and C3da neurons act downstream of
162 epidermal cells to drive behaviors. We note that TnT expression in C4da neurons did not completely block epidermis-evoked nocifensive behaviors, and this likely reflects
164 both incomplete C4da neuron silencing and epidermal activation of other SSNs that promote nociceptive outputs including C3da neurons, C2da neurons, and Cho neurons
166 (Ohyama *et al.*, 2015; Hu *et al.*, 2017; Burgos *et al.*, 2018). Further, silencing C4da or C3da neurons while stimulating epidermal cells led to an increase in the non-
168 nocifensive behaviors hunching and freezing (Fig. 3E, 3F). These results, along with the observation that rolling behaviors predominate the early behavioral responses to
170 epidermal stimulation (Fig. 2B), suggest that the nervous system prioritizes nocifensive behavioral outputs following epidermal stimulation. These data support a model in which
172 epidermal cells and SSNs are functionally coupled.

174 ***Epidermal stimulation potentiates nociceptive neurons and behaviors***

What is the physiological relevance of this functional coupling of epidermal cells and
176 SSNs? To address this question, we compared calcium responses in C4da neurons to either simultaneous epidermal and C4da optogenetic stimulation or C4da stimulation
178 alone. Simultaneous stimulation significantly enhanced the magnitude and duration of calcium responses in C4da axons (Fig. 4A-4D, 4S1). Based on this prolonged calcium
180 response, we hypothesized that simultaneous epidermis and C4da neuron stimulation would yield enhanced nocifensive behavior output. To test this, we stimulated C4da
182 neurons and epidermal cells individually or in combination using low intensity CsChrimson activation and monitored larval behavior responses. In this stimulation
184 paradigm, simultaneous epidermal cell and C4da neuron stimulation resulted in rolling in 100% of larvae whereas selective stimulation of C4da neurons or epidermal cells
186 induced rolling in only 63% or 18% of larvae, respectively (Fig. 4E, 4F). Furthermore, simultaneous stimulation elicited a significantly higher number of rolls among
188 responders than stimulation of nociceptors or epidermal cells alone (26.9 rolls for C4da + Epi, 4.9 for C4da, and 5.3 for Epi stimulation; Fig 4G, 4H). Likewise, simultaneous
190 stimulation significantly reduced the latency to the first roll (Fig. 4I) and increased the

duration of rolling behaviors (Fig. 4J). We next tested whether this functional coupling
192 extends to mechanical stimuli. We simultaneously presented larvae with a noxious mechanical stimulus and a low intensity optogenetic epidermal stimulus that was
194 insufficient to trigger rolling on its own (0% response rate, n = 200, data not shown). This concurrent epidermal stimulation significantly increased touch-evoked nocifensive
196 responses, yielding a 91% or 49% increase in rolling responses to 20 mN or 50 mN Von Frey stimulus, respectively (Fig. 4K). We next probed the kinetics of this epidermis-
198 induced mechanical sensitization.

When *Drosophila* larvae are presented with two nociceptive mechanical stimuli in
200 succession, they exhibit enhanced behavioral responses to the second stimulus (Hu *et al.*, 2017). We hypothesized that selective epidermal stimulation would sensitize larvae
202 to subsequent nociceptive mechanical stimuli. To test this hypothesis, larvae expressing the warmth-activated calcium-permeable channel dTRPA1 in epidermal cells were
204 presented with a thermal stimulus, 32º C to activate dTRPA1, followed by a 40 mN mechanical stimulus 10 sec later (Fig. 4L). Indeed, we found that dTRPA1-mediated
206 epidermal stimulation significantly sensitized larvae to a subsequent mechanical stimulus, increasing the roll probability more than two-fold. In contrast, dTRPA1-
208 mediated stimulation of C4da neurons did not induce mechanical sensitization (Fig. 4L). Thus, activation of epidermal cells but not C4da nociceptors alone is sufficient to induce
210 prolonged sensitization to noxious mechanical stimuli. We next assessed the duration of sensitization following transient epidermal activation. Thermogenetic epidermal
212 stimulation yielded persistent sensitization that recovered over a timescale of minutes (τ = 337 sec, Fig. 4M, 4N). The magnitude and duration of mechanical sensitization by
214 thermogenetic epidermal stimulation was remarkably similar to the sensitization evoked by a prior mechanical stimulus (63% roll probability in response to a second stimulus, τ
216 = 334 sec, Fig. 4N, 4S1B). Altogether our data support a model whereby epidermal cells are mechanosensitive cells that signal to SSNs to drive acute nocifensive behaviors and
218 prolong mechanical sensitization.

220 ***Epidermal cells are intrinsically mechanosensitive***

Prior studies have shown that vertebrate epidermal cells directly respond to mechanical
222 stimuli (Koizumi *et al.*, 2004; Haeberle *et al.*, 2008; Tsutsumi *et al.*, 2009; Ranade *et al.*, 2014; Woo *et al.*, 2014; Moehring *et al.*, 2018). Therefore, we next assessed whether
224 *Drosophila* epidermal cells are intrinsically mechanosensitive. We developed a protocol to acutely dissociate epidermal cells and measure the responses of individual
226 GCaMP6s-expressing epidermal cells to mechanical stimuli (Fig. 5A). We found that radial stretch elicits calcium responses in epidermal cells in a dose-dependent manner.
228 For example, a low 0.5% stretch activated 18% of cells and a subsequent 1% stretch recruited an additional 10% of stretch-responding cells (Fig. 5B-5D). Overall, 51% of
230 epidermal cells displayed stretch sensitivity (Fig. 5C, 5D). We also found that 43% of epidermal cells responded to hypoosmotic challenge and 35% responded to laminar
232 flow; 19% of epidermal cells responded to both hypoosmotic challenge and laminar flow (Fig. 5S1). Given that dissociated epidermal cells were intrinsically mechanosensitive,
234 we next assessed mechanically evoked responses in a semi-intact body wall preparation (Fig. 5E). We found that 50% of epidermal cells exhibited a robust calcium
236 transient in response to a 25 µm membrane displacement using a glass probe (Fig. 5E-5G, 5S1G). Altogether, these results indicate that *Drosophila* larval epidermal cells are
238 intrinsically mechanosensitive.

240 ***Mechanically evoked epidermal responses rely on store-operated calcium entry***

Our studies demonstrate that, like vertebrate keratinocytes, *Drosophila* epidermal cells
242 exhibit mechanically evoked calcium transients. What is the mechanism of mechanotransduction in these cells? RNA-seq analysis of acutely dissociated epidermal
244 cells revealed expression of more than 20 cation channels, including the mechanosensitive ion channels Piezo, TMEM63, and TMCO (Fig. 6S1). We assessed
246 the requirement of these channels in epidermal control of mechanical nociception using available RNAi transgenes (Fig. 6A). Our behavioral screen identified one channel,
248 *Orai*, the sole *Drosophila* pore-forming subunit of the Ca^{2+} release-activated Ca^{2+} (CRAC) channel (Feske *et al.*, 2006), that blocked sensitization without impacting
250 behavioral responses to the first stimulus (Fig. 6A, 6B, 6S2A). While our RNAi studies

did not reveal an epidermal requirement for any known mechanosensitive cation
252 channels in mechanonociceptive behaviors, it is possible that multiple channels function redundantly, or that RNAi knockdown was incomplete. Interestingly, our screen
254 additionally uncovered a role for *Task6*, an orthologue of stretch-sensitive 2-pore potassium channels (Fink *et al.*, 1996), in epidermal control of mechanonociception, as
256 *Task6* RNAi increased nocifensive rolling responses to the initial mechanical stimulus (Fig. 6S2B).

258 To gain insight into mechanically evoked nociceptive sensitization, we focused on probing the role of Orai in epidermal mechanosensory responses. We first asked
260 whether Orai is functional in *Drosophila* epidermal cells. Orai is a store-operated calcium (SOC) channel that is activated by the endoplasmic reticulum (ER)-calcium
262 sensitive molecule, Stim, upon calcium release from ER calcium stores. Thapsigargin (TG) induces calcium release from intracellular stores and thus triggers activation of
264 Orai channels. Indeed, *Drosophila* epidermal cells displayed TG-induced calcium release in the absence of extracellular calcium, followed by calcium influx upon re-
266 addition of extracellular calcium (Fig. 6C). Calcium influx was significantly inhibited by the addition of low nanomolar lanthanum, consistent with the high sensitivity of Orai
268 channels to lanthanides (Fig. 6S2C). This characteristic store operated calcium entry (SOCE) response was significantly reduced by epidermis-specific *Stim* or *Orai* RNAi
270 knockdown (Fig. 6S2D-F). Given that Stim and Orai mediate SOCE, we investigated requirements for epidermal Stim and Orai in mechanically evoked calcium responses.
272 We found that RNAi knockdown of either *Stim* or *Orai* significantly reduced the fraction of stretch-responsive epidermal cells (RNAi control = 48%, *Stim* RNAi = 22%, *Orai* RNAi
274 = 24%; Fig. 6D-E), and that *Stim* or *Orai* RNAi preferentially attenuated stretch evoked responses to larger magnitude stretch stimuli. Likewise, stretch evoked responses were
276 attenuated in the presence of the Orai blocker lanthanum chloride, or when intracellular stores were depleted by TG, suggesting that both store release and calcium influx
278 contribute to the epidermal stretch response (Fig. 6F-G). We also found that human keratinocytes display dose-dependent stretch evoked calcium responses, though they
280 respond to higher magnitudes of stretch than *Drosophila* epidermal cells (Fig. 6H). Like

Drosophila, both store release and calcium influx contribute to stretch evoked calcium
282 responses in human keratinocytes (Fig. 6I).

Two hallmarks of Stim and Orai-mediated SOCE are steep inward rectification,
284 with larger currents at hyperpolarizing potentials, and highly cooperative Orai activation by Stim (Hoover and Lewis, 2011). Since Stim and Orai mediate mechanical responses
286 of epidermal cells *in vitro*, we predicted that increasing the calcium driving force through Orai activity by either hyperpolarizing epidermal cells or by activating additional Orai
288 channels via *Stim* overexpression would enhance behavioral responses to mechanical stimuli. Indeed, we found that hyperpolarizing epidermal cells with the light-activated
290 anion channelrhodopsin GtACR1 (Mohammad *et al.*, 2017) increased behavioral responses to mechanical stimuli (Fig. 6J). In addition, overexpressing *Stim* in epidermal
292 cells significantly enhanced nocifensive behavioral responses to mechanical stimuli (Fig. 6K). Altogether, these results demonstrate that mechanically evoked responses of
294 epidermal cells and the resulting nocifensive behavior outputs require store-operated calcium entry.

296 How might mechanically evoked calcium entry in epidermal cells drive nociceptor activation and behavior? Stim/Orai-mediated calcium entry contributes to exocytosis in
298 a variety of cell types, including neurons and immune cells (Pores-Fernando and Zweifach, 2009; Ashmole *et al.*, 2012; Maneshi *et al.*, 2020; Chanaday *et al.*, 2021;
300 Ramesh *et al.*, 2021). Therefore, we investigated the contribution of epidermal exocytosis in nociceptive sensitization with the temperature-sensitive dynamin mutant
302 *shibire*^{ts} (*shi*^{ts}) to inducibly block vesicle recycling, as this treatment rapidly and potently blocks neurotransmitter release (Koenig *et al.*, 1983). In this paradigm, larvae
304 expressing *shi*^{ts} in epidermal cells, but not control larvae, exhibited significant attenuation of mechanically evoked nociceptive sensitization following pre-incubation at
306 the non-permissive temperature (Fig. 6L). In contrast, both genotypes exhibited comparable responses to a mechanical stimulus at the permissive temperature (25° C)
308 and to the first mechanical stimulus following pre-incubation at the non-permissive temperature (30° C). Taken together, these results are consistent with a model in which
310 mechanical stimuli induce calcium influx and vesicular release from epidermal cells,

which in turn activates nociceptors to induce acute nocifensive behaviors and prolonged
312 sensitization (Fig. 6M).

314 **Discussion**

In this study, we have shown an essential role for *Drosophila* epidermal cells in
316 escape responses to noxious mechanical stimuli. Activation of epidermal cells acutely activates SSNs to induce an array of behavioral outputs and mechanical sensitization.
318 This epidermal potentiation persists for minutes to promote a prolonged, but reversible, mechanical hypersensitivity that may protect from further insult. This is distinct from
320 previously described forms of neuropathic thermal and mechanical hypersensitivity in *Drosophila* which are induced by tissue damage and chemotherapuetic agents,
322 respectively, emerge on a timescale of hours, and are long-lasting (Babcock *et al.*, 2009; Boiko *et al.*, 2017; Khuong *et al.*, 2019). In the mammalian somatosensory
324 system, a variety of inflammatory mediators have been shown to activate TRPA1 in neurons to promote mechanical hypersensitivity (Bautista *et al.*, 2006); however, the
326 molecular force transducers that mediate mechanical pain are unknown. In contrast, in the *Drosophila* somatosensory system, *Ppk1*/*Ppk26*, *Piezo*, and *Trpa1* are key
328 transducers of mechanonociception (Kim *et al.*, 2012b; Gorczyca *et al.*, 2014; Guo *et al.*, 2014; Mauthner *et al.*, 2014). Prolonged sensitization to noxious mechanical stimuli
330 plays an important protective role in an organism's survival; yet the mechanisms of mechanical sensitization of *Drosophila* nociceptors were unknown.

332 We demonstrate a new role for SOC signaling in both *Drosophila* and human epidermal cell mechanotransduction. While short-term sensitization is beneficial to
334 survival, a key hallmark of pathological pain is prolonged and persistent mechanical hypersensitivity; whether deregulation of this mechanism of epidermis-evoked short-
336 term sensitization contributes to pathological pain remains to be determined. Overall, we identified a mechanism that does not impact acute nociception but selectively
338 regulates mechanical sensitization. These findings highlight Stim/Orai signaling as a new avenue for understanding mechanical pain.

340 This work has opened several new directions for future studies. First, how does radial and osmotic stretch lead to the activation of store-operated calcium signaling? 342 Although Orai has not previously been shown to be mechanosensitive, our studies revealed a requirement for Orai and its activator Stim in mechanically-evoked calcium 344 flux in *Drosophila* epidermal cells. We also showed that radial stretch of human keratinocytes triggered calcium release from stores and SOCE; our previous studies 346 showed that Stim and Orai are required for SOCE in human keratinocytes (Wilson *et al.*, 2013). These data in combination with previous findings that showed mechanical 348 stimulation of human mesenchymal stem cells also triggers SOCE (Kim *et al.*, 2015) suggests that Stim/Orai signaling may represent a conserved pathway for 350 mechanotransduction in non-neuronal cells.

Second, how is Stim/Orai function linked to mechanotransduction? Stim/Orai 352 signaling is activated downstream of G-protein coupled receptors (GPCRs) and receptor tyrosine kinases (RTKs) through phospholipase C. Studies have shown that a number 354 GPCRs are mechanosensitive (Chachisvilis *et al.*, 2006; Grosmaitre *et al.*, 2007; Mederos y Schnitzler *et al.*, 2008; Connelly *et al.*, 2015; Xu *et al.*, 2018), though this has 356 not been studied in epidermal cells. Alternatively, plasma membrane deformation has been shown to induce ER-plasma membrane junctions (Venturini *et al.*, 2020; Aoki *et* 358 *al.*, 2021), where Stim and Orai clusters accumulate and interact to drive calcium influx (Luik *et al.*, 2008).

360 Third, how does mechanically-induced singaling in epidermal cells lead to modulation of SSNs? Our data support a model whereby epidermal cells and multiple 362 classes of SSNs are functionally coupled. Epidermal stimulation directly activates nociceptive C4da neurons and mechanosensory C3da and Cho neurons, and the output 364 of neuronal activity is required for epidermis-evoked behaviors. Furthermore, we demonstrated a requirement for dynamin-dependent vesicle release from epidermal 366 cells in mechanical sensitization, providing a potential link between Stim/Orai signaling in epidermal cells and downstream neuronal activity. However, the mediators that are 368 released by epidermal cells and the signaling molecules in the nociceptors remain unknown.

370 Which epidermal-derived molecules might modulate neuronal activity? There are
several mechanisms by which mammalian epidermal cells activate SSNs. Vesicular
372 release of norepinephrine from mouse epidermal Merkel cells is required for sustained
touch-evoked firing of mechanosensory neurons (Hoffman *et al.*, 2018). Additionally,
374 mechanical stimuli trigger ATP release from mouse keratinocytes that activates
nociceptors via purinergic (P2X4) receptors (Koizumi *et al.*, 2004; Tsutsumi *et al.*, 2009;
376 Moehring *et al.*, 2018). Finally, Stim/Orai-dependent SOCE mediates the release of the
cytokine thymic stromal lymphopoietin (TSLP) from keratinocytes that directly activates
378 a subset of TRPA1-expressing SSNs to induce itch (Wilson *et al.*, 2013). Similar to
these mammalian models, UV-damage has been shown to induce the release of the
380 cytokine Eiger to promote nociceptor sensitization (Babcock *et al.*, 2009); though this
occurred on a slower timescale than the epidermal-evoked mechanical sensitization we
382 describe here (8 hrs vs. ~ 10 sec, Fig. 4L). Likewise, epidermal platelet-derived growth
factor (PDGF) ligands regulate mechanonociceptive responses in *Drosophila* (Lopez-
384 Bellido *et al.*, 2019) and intrathecal delivery of PDGF or the closely related growth factor
EGFR yields mechanical hypersensitivity in rats (Masuda *et al.*, 2009; Puig *et al.*, 2020),
386 but it remains to be determined whether growth factor signaling can yield rapid
sensitization. Hence, future studies will address which neurotransmitters,
388 neuropeptides, or inflammatory mediators underly epidermal cell-mediated mechanical
sensitization.

390 Our data support a model whereby epidermal cells and multiple classes of SSNs
are functionally coupled. Future studies will address which neurotransmitters,
392 neuropeptides, or inflammatory mediators underly epidermal cell-mediated mechanical
sensitization. An additional key next step is understanding whether the neuronal
394 plasticity underlying mechanical sensitization results from the direct modulation of
mechanosensitive channels or rapid insertion of new mechanosensitive channels into
396 the plasma membrane, or from changes in the signaling pathways or channels that
regulate neuronal excitability. Overall, we performed an unbiased genetic screen that for
398 the first time establishes a key role for mechanically-evoked Stim/Orai calcium signaling
in epidermal cells that drive nociceptor modulation and mechanical hypersensitivity.

400

Material and Methods

402 ***Drosophila strains***

Flies were maintained on standard cornmeal-molasses-agar media and reared at 25° C
404 under 12 h alternating light-dark cycles. For all experiments involving optogenetic manipulations, larvae were raised in the constant dark at 25 °C on Nutri-Fly Instant
406 Food (Genesee Scientific #66-117), supplemented with 1 mM all-trans retinal (ATR; Sigma #R2500). See Table S1 for a complete list of alleles used in this study.
408 Experimental genotypes are listed in figure legends.

410 **Behavior analysis**

Optogenetic behavior screen

412 Individual larvae were rinsed in ddH2O, transferred to an agarose substrate (1% agarose, 100 mM dish) in a darkened arena, and habituated for 30 sec. Larvae were
414 stimulated with a top-mounted 488 nM LED illuminator (PE-300, CoolLED) and images were captured with a sCMOS camera (Orca Flash 3.0, Hamamatsu) at frame
416 acquisition rate of 20 fps and behaviors were scored before, during and after optogenetic stimulation.

418

High resolution video tracking of optogenetic-gated larval behavior

420 Following 5 min of light deprivation including 15 sec of habituation in the behavioral arena, larvae were tracked before, during and after optical stimulus (10 sec each, 30
422 sec total) (Fig. 2A). For these studies we modified our stimulation paradigm in two key ways: to avoid potential contributions of nociceptor light evoked responses (Xiang *et al.*,
424 2010), we stimulated larvae using yellow-shifted light; and to facilitate kinetic analysis of behavior outputs, we used an automated shutter. Larvae were stimulated with a top-
426 mounted 585 nm LED illuminator (SPECTRA X, Lumencor) equipped with a filter (FF01 585/40-25, Semrock), and images were captured with a sCMOS camera (Zyla4.2,
428 Andor) at a frame rate of 20Hz. Larvae were constantly illuminated with an infrared (940

nm) light source (LDR2-132IR2-940-LA, CSS) for visualization. Larvae were fed (ATR+)
430 or vehicle alone (ATR-) as indicated.

432 *Thermogenetic behavior assays*

Larvae for thermogenetic assays were reared at room temperature (20° C) to limit
434 TRPA1 activation during development. Third instar larvae were isolated from their food, washed in distilled water, and recovered to damp agar plates for several min, and
436 transferred individually to a Peltier plate held at 25° C or 35° C. Behavior responses were recorded under infrared light with a computer-controlled GigE camera (FLIR) at an
438 acquisition rate of 20 fps for 20 sec. Responses were analyzed post-hoc blind to genotype and were plotted as the proportion of larvae that exhibited at least one
440 complete nocifensive roll during stimulus application.

442 *Mechanonociception assays*

Third instar larvae were isolated from their food, washed in distilled water, and placed
444 on a scored 35 mm petri dish with a thin film of water such that larvae stayed moist but did not float. Larvae were stimulated dorsally between segments A4 and A7 with
446 calibrated Von Frey filaments that delivered the indicated force upon buckling, and nocifensive rolling responses were scored during the 10 sec following stimulus removal.
448 For assays involving multiple stimuli, larvae were stimulated individually, allowed to freely locomote in the arena for up to 1 min (for longer recoveries larvae were recovered
450 onto 2% agar to prevent desiccation), and subsequently presented with the second stimulus. For assays involving thermal and mechanical stimuli, larvae were individually
452 transferred to a pre-warmed Peltier plate containing a thin layer of water, incubated for the indicated time, and transferred to the behavior arena (or a 2% agar plate for
454 recoveries > 1 min) with a paint brush for subsequent mechanical stimulation. All assays were conducted in ambient light except for experiments with GtACR (Fig. S72), which
456 were conducted under broad-spectrum (500-700 nm) LED illumination (CoolLED PE-300, green). Our illumination setup for these experiments provided limited working
458 distance, therefore larvae were restrained with forceps and given only a single stimulus.

460 *Video annotations*

Videos of individual larvae responding to light stimuli were scored on a frame-by-frame
462 basis using the annotation software BORIS (Friard and Gamba, 2016). Behaviors scored, along with descriptions of the criteria for each behavior, are detailed in Table
464 S2. Video analysts were blind to the genotype and treatment during scoring. Scoring on a training set was compared across all analysts to calibrate, and any behaviors for
466 which the primary analyst was uncertain were reviewed by an additional analyst. Additionally, 10% of videos were scored independently by two analysts and there was at
468 least 80% concordance in behaviors annotated in these comparisons.

470 **Microscopy**

Calcium imaging: ventral nerve cords

472 Third-instar larvae were dissected along the dorsal midline and pinned on a sylgard-coated dish (Silpot 184, Dow Corning Toray). The internal organs except for neural
474 tissues were removed. Larvae were bathed in HL3.1 (Feng et al, 2004) modified to remove calcium (Table S3) to minimize larval movement. The ventral nerve cord was
476 imaged using an Olympus BX51WI microscope, equipped with a spinning-disk confocal unit Yokogawa CSU10 (Yokogawa) and an EM-CCD digital camera (Evolve,
478 Photometrics). For activation of epidermal cells with the light gated CsChrimson, red light was delivered by a pE-300 (CoolLED) equipped with a filter (ET645/30x, Chroma).
480 Obtained images were analyzed using Metamorph (https://www.moleculardevices.com/systems/metamorph-research-imaging) and ImageJ
482 (Schneider *et al.*, 2012). Baseline fluorescence was calculated as the mean fluorescence intensity of an ROI over the ten frames prior to light stimulus delivery. The
484 trapezoidal method was used to calculate area under the curve, utilizing the trapz function of MATLAB. Data points from the onset of stimulation to the end of stimulation
486 were used for the calculation.

488 *Calcium imaging: fillet preparations*

Third-instar larvae were dissected along the ventral midline and pinned on sylgard (Dow
490 Corning) dishes with the internal surface facing towards the microscope. All internal organs, including the central nervous system, were removed. Larvae were bathed in
492 calcium-containing HL3.1 (Feng *et al.*, 2004) (Table S3) except where indicated and images of the dorsal midline between abdominal segments A2 and A4 were captured
494 with a Zeiss Axio Zoom V16 microscope. Captured images were analyzed using ImageJ (Schneider *et al.*, 2012). Mechanical stimulus: fillets were poked with a tapered
496 borosilicate capillary with a rounded tip, using a micromanipulator to induce a deflection of 25 μm. The decay time constant was calculated by fitting the data points from the
498 peak response to the end of the experiment into an exponential curve f(x) = a*exp(b*x) using MATLAB with R^2>0.9 used as a threshold for reliable fitting.
500

Calcium imaging: dissociated epidermal cells

502 Six to eight larval fillets were dissociated in 400 μL of 50% Saline (modified Ringer's recipe) / 50% Schneider's media with 200 U/mL collagenase type I (Fisher 17-100-017),
504 with mixing at 1000 RPM at 33°C for 16 min, with trituration every 8 min. Undigested fillets were removed and the remaining suspension was spun at 500 g for 3 min,
506 followed by aspiration of the supernatant down to a 10 μL cell suspension. Cells were resuspended in 30 μL fresh PBS / Schneider's solution and plated onto poly-D-lysine (1
508 mg/ml, Sigma P7886) coated No. 1 coverslips, with 10 μL cell solution per coverslip. Cells were cultured at least 30 min and up to 2 hr at 25° C prior to imaging. Cells were
510 imaged using a a 10x objective at a frame rate of 0.33 Hz. Solutions are indicated in figure legends (see Table S3 for recipes). Obtained images were analyzed using
512 MetaFluor and Python and baseline fluorescence was calculated as the mean fluorescence intensity of an ROI over 5 frames prior to stimulus delivery. For stretch
514 stimulation, circular membranes were cut with an arch punch from sheets of glossy silicone of 0.01–0.02 inch thickness (Specialty Manufacturing, Inc.) and coated with 1
516 mg/ml poly-D-lysine for 1 h before plating cells. Membranes were mounted onto the StageFlexer system and vacuum pressure was applied through the FX-3000 system
518 (Flexcell). Calibrations were performed using fluorescent beads attached to the

membranes, and images were taken before and during a static stretch. To stimulate
520 cells, a 2 sec square wave of vacuum pressure was applied. Cells were imaged with an Olympus BX61WI upright microscope. For store-operated calcium entry measurements
522 and osmotic stimulation, cells were imaged using a Zeiss Observer inverted microscope and solutions were perfused using the Automate Scientific ValveLink 8.2 perfusion
524 system. At the end of each imaging session, 1uM ionomycin was perfused and only cells that showed a calcium response, as defined by a 10% increase from baseline
526 fluorescence, were used in analysis. Flow, osmotic and radial stretch responders were defined by a 5% increase from baseline fluorescence.
528

Calcium imaging: human keratinocytes

530 Immortalized human keratinocytes (HaCaT) cells were plated on silicone membranes one day prior to stretch experiments. Prior to the radial stretch experiments, cells were
532 loaded with 1 µm Fura-2AM supplemented with 0.01% Pluronic F-127 (w/v, Life Technologies) in a physiological Ringer's solution containing the following (in mm): 140
534 NaCl, 5 KCl, 10 HEPES, 2 $CaCl_2$, 2 $MgCl_2$, and 10 d-(+)-glucose, pH 7.4. Acquired images were displayed as the ratio of 340 nm/380 nm. Cells that had a response 10
536 standard deviations above baseline to ionomycin were included in the analysis and stretch responses were defined by a 15% increase in Fura-2 340/380 ratio.
538

Confocal Microscopy

540 For peripheral imaging of cellular morphology, live single larvae were mounted in 90% glycerol under a coverslip and imaged on a Leica SP5 confocal microscope using a 40x
542 1.25 NA lens. To image the larval CNS, larvae were dissected on sylgard plates, briefly fixed in 4% paraformaldehyde (PFA) in PBS for 15 min at room temperature, washed 3
544 x 5 min in PBS, and mounted for imaging.

546 **RNA-Seq analysis of epidermal cells**

RNA isolation for RNA-Seq

548 Larvae with cytoplasmic GFP expressed in different epidermal subsets were microdissected and dissociated in collagenase type I (Fisher 17-100-017) into single cell
550 suspensions, largely as previously described (Williams *et al.*, 2016), with the addition of 1% BSA to the dissociation mix. After dissociation, cells were transferred to a new 35
552 mm petri dish with 1 mL 50% Schneider's media, 50% PBS supplemented with 1% BSA. Under a fluorescent stereoscope, individual fluorescent cells were manually
554 aspirated with a glass pipette into PBS with 0.5% BSA, and then serially transferred until isolated without any additional cellular debris present. Ten cells per sample were
556 aspirated together, transferred to a mini-well containing 3ul lysis solution (0.2 % Triton X-100 in water with 2 U / μL RNAse Inhibitor), lysed by pipetting up and down several
558 times, transferred to a microtube, and stored at -80° C. For the picked cells, 2.3 μL of lysis solution was used as input for library preparation.

560

RNA-Seq library preparation

562 RNA-Seq libraries were prepared from the picked cells following the Smart-Seq2 protocol for full length transcriptomes (Picelli *et al.*, 2014). To minimize batch effects,
564 primers, enzymes, and buffers were all used from the same lots for all libraries. Libraries were multiplexed, pooled, and purified using AMPure XP beads, quality was
566 checked on an Agilent TapeStation, and libraries were sequenced as 51-bp single end reads on a HiSeq4000 at the UCSF Center for Advanced Technology.

568

RNA-Seq data analysis

570 Reads were demultiplexed with CASAVA (Illumina) and read quality was assessed using FastQC (https://www.bioinformatics.babraham.ac.uk/) and MultiQC (Ewels *et al.*,
572 2016). Reads containing adapters were removed using Cutadapt version 2.4 (Martin, 2011) and reads were mapped to the *D. melanogaster* transcriptome, FlyBase genome
574 release 6.29, using Kallisto version 0.46.0 (Bray *et al.*, 2016) with default parameters. AA samples were removed from further analysis for poor quality, including low read
576 depth (< 500,000 reads), and low mapping rates (< 80%). Raw sequencing reads and

gene expression estimates are available in the NCBI Sequence Read Archive (SRA)
578 and in the Gene Expression Omnibus (GEO) under accession number SUB11489996.

580 **Statistical analysis**

For each experimental assay control populations were sampled to estimate appropriate
582 sample numbers to allow detection of ~33% differences in means with 80% power over a 95% confidence interval. Details of statistical tests including treatment groups, sample
584 numbers, statistical tests, p-values and q-values are provided in the experimental supplement.

586

Acknowledgements

588 This work was supported by grants from the National Institutes of Health to J.Z.P. (NINDS R01 NS076614), DB (NICHD K99 HD086271), CW (5F31NS106775), and the
590 MBL (R25NS063307); a grant from the National Science Foundation to S.S.M (NSF GRFP DGE1752814); a grant from the Weill Neurohub to J.Z.P and D.B.; a grant from
592 the Scan Design Foundation, a JSPS long-term fellowship and startup funds from UW (J.Z.P); MEXT Grants-in-Aid for Scientific Research (KAKENHI 16H06456), JSPS
594 (KAKENHI 16H02504), WPI-IRCN, AMED-CREST (JP22gm310010), and JST-CREST to KE; and a fellowship from the Grass Foundation (C.E.E.). Fly Stocks obtained from
596 the Bloomington *Drosophila* Stock Center (NIH P40OD018537) were used in this study. We thank Jessica Huang, Jordan Martel, and David Shen for assistance with video
598 tracking; Peter Soba for helpful discussions.

600 **Author Contributions**

Conception and design: Optogenetic behavior analysis, K.E., J.Z.P, C.R.W, J.Y.; larval
602 behavior assays, J.Z.P, C.R.W, and J.Y.; in vivo calcium imaging, K.E., J.Z.P, C.R.W, J.Y.; ex vivo calcium imaging, D.B., S.S.M., and J.Z.P

604 *Acquisition of data*: Optogenetic behavior screen, C.J.A, C.E.E., S.M., and J.Y.; Optogenetic behavior assays, J.Y., C.H., M.M., K.I., and C.R.W.; mechanonociception

606 assays, C.R.W, and J.Z.P; thermogenetic behavior assays, J.Z.P.; RNA-sequencing, J.Z.P. and C.R.W.

608 *Analysis and Interpretation of data*: larval behavior assays, J.Z.P, C.R.W, J.Y.; in vivo calcium imaging, K.E., J.Z.P, C.R.W, J.Y.; ex vivo calcium imaging, D.B. and S.S.M.;
610 transcriptomic data, C.H., C.R.W., and J.Z.P.

Drafting the article: D.B., J.Z.P, C.R.W, S.S.M., and J.Y.

612

Competing Interests

614 DMB is on the scientific advisory board of Escient Pharmaceuticals. The remaining authors declare no conflicts of interest.

616

References

618 Aoki, K, Harada, S, Kawaji, K, Matsuzawa, K, Uchida, S, and Ikenouchi, J (2021). STIM-Orai1 signaling regulates fluidity of cytoplasm during membrane blebbing. Nat Commun
620 12, 480.

Ashmole, I, Duffy, SM, Leyland, ML, Morrison, VS, Begg, M, and Bradding, P (2012).
622 CRACM/Orai ion channel expression and function in human lung mast cells. J Allergy Clin Immunol 129, 1628-1635.e2.

624 Babcock, DT, Landry, C, and Galko, MJ (2009). Cytokine signaling mediates UV-induced nociceptive sensitization in Drosophila larvae. Curr Biol 19, 799–806.

626 Bautista, DM, Jordt, S-E, Nikai, T, Tsuruda, PR, Read, AJ, Poblete, J, Yamoah, EN, Basbaum, AI, and Julius, D (2006). TRPA1 mediates the inflammatory actions of
628 environmental irritants and proalgesic agents. Cell 124, 1269–1282.

Boiko, N et al. (2017). TrpA1 activation in peripheral sensory neurons underlies the ionic
630 basis of pain hypersensitivity in response to vinca alkaloids. PLoS ONE 12, e0186888.

Bray, NL, Pimentel, H, Melsted, P, and Pachter, L (2016). Near-optimal probabilistic
632 RNA-seq quantification. Nat Biotechnol 34, 525–527.

Burgos, A et al. (2018). Nociceptive interneurons control modular motor pathways to
634 promote escape behavior in Drosophila. Elife 7.

Cauna, N (1973). The free penicillate nerve endings of the human hairy skin. J Anat
636 115, 277–288.

Chachisvilis, M, Zhang, Y-L, and Frangos, JA (2006). G protein-coupled receptors
638 sense fluid shear stress in endothelial cells. Proc Natl Acad Sci U S A 103, 15463–
15468.

640 Chalfie, M, and Sulston, J (1981). Developmental genetics of the mechanosensory
neurons of Caenorhabditis elegans. Dev Biol 82, 358–370.

642 Chanaday, NL, Nosyreva, E, Shin, O-H, Zhang, H, Aklan, I, Atasoy, D, Bezprozvanny, I,
and Kavalali, ET (2021). Presynaptic store-operated Ca2+ entry drives excitatory
644 spontaneous neurotransmission and augments endoplasmic reticulum stress. Neuron
109, 1314-1332.e5.

646 Chung, M-K, Lee, H, Mizuno, A, Suzuki, M, and Caterina, MJ (2004). TRPV3 and
TRPV4 mediate warmth-evoked currents in primary mouse keratinocytes. J Biol Chem
648 279, 21569–21575.

Connelly, T, Yu, Y, Grosmaitre, X, Wang, J, Santarelli, LC, Savigner, A, Qiao, X, Wang,
650 Z, Storm, DR, and Ma, M (2015). G protein-coupled odorant receptors underlie
mechanosensitivity in mammalian olfactory sensory neurons. Proc Natl Acad Sci U S A
652 112, 590–595.

Ewels, P, Magnusson, M, Lundin, S, and Käller, M (2016). MultiQC: summarize analysis
654 results for multiple tools and samples in a single report. Bioinformatics 32, 3047–3048.

Feng, Y, Ueda, A, and Wu, C-F (2004). A modified minimal hemolymph-like solution,
656 HL3.1, for physiological recordings at the neuromuscular junctions of normal and mutant
Drosophila larvae. J Neurogenet 18, 377–402.

658 Feske, S, Gwack, Y, Prakriya, M, Srikanth, S, Puppel, S-H, Tanasa, B, Hogan, PG,
Lewis, RS, Daly, M, and Rao, A (2006). A mutation in Orai1 causes immune deficiency
660 by abrogating CRAC channel function. Nature 441, 179–185.

Fink, M, Duprat, F, Lesage, F, Reyes, R, Romey, G, Heurteaux, C, and Lazdunski, M
662 (1996). Cloning, functional expression and brain localization of a novel unconventional
outward rectifier K+ channel. EMBO J 15, 6854–6862.

664 Friard, O, and Gamba, M (2016). BORIS: a free, versatile open-source event-logging
software for video/audio coding and live observations. Methods in Ecology and
666 Evolution 7, 1325–1330.

Galko, MJ, and Krasnow, MA (2004). Cellular and genetic analysis of wound healing in
668 Drosophila larvae. PLoS Biol 2, E239.

Gorczyca, DA, Younger, S, Meltzer, S, Kim, SE, Cheng, L, Song, W, Lee, HY, Jan, LY,
670 and Jan, YN (2014). Identification of Ppk26, a DEG/ENaC Channel Functioning with

Ppk1 in a Mutually Dependent Manner to Guide Locomotion Behavior in Drosophila. Cell Rep 9, 1446–1458.

Grosmaitre, X, Santarelli, LC, Tan, J, Luo, M, and Ma, M (2007). Dual functions of mammalian olfactory sensory neurons as odor detectors and mechanical sensors. Nat Neurosci 10, 348–354.

Guo, Y, Wang, Y, Wang, Q, and Wang, Z (2014). The role of PPK26 in Drosophila larval mechanical nociception. Cell Rep 9, 1183–1190.

Haeberle, H, Bryan, LA, Vadakkan, TJ, Dickinson, ME, and Lumpkin, EA (2008). Swelling-activated Ca2+ channels trigger Ca2+ signals in Merkel cells. PLoS One 3, e1750.

Hamada, FN, Rosenzweig, M, Kang, K, Pulver, SR, Ghezzi, A, Jegla, TJ, and Garrity, PA (2008). An internal thermal sensor controlling temperature preference in Drosophila. Nature 454, 217–220.

Han, C, Wang, D, Soba, P, Zhu, S, Lin, X, Jan, LY, and Jan, Y-N (2012). Integrins regulate repulsion-mediated dendritic patterning of drosophila sensory neurons by restricting dendrites in a 2D space. Neuron 73, 64–78.

Hoffman, BU, Baba, Y, Griffith, TN, Mosharov, EV, Woo, S-H, Roybal, DD, Karsenty, G, Patapoutian, A, Sulzer, D, and Lumpkin, EA (2018). Merkel Cells Activate Sensory Neural Pathways through Adrenergic Synapses. Neuron 100, 1401-1413.e6.

Hoover, PJ, and Lewis, RS (2011). Stoichiometric requirements for trapping and gating of Ca2+ release-activated Ca2+ (CRAC) channels by stromal interaction molecule 1 (STIM1). Proc Natl Acad Sci U S A 108, 13299–13304.

Hu, C et al. (2017). Sensory integration and neuromodulatory feedback facilitate Drosophila mechanonociceptive behavior. Nat Neurosci 20, 1085–1095.

Hwang, RY, Zhong, L, Xu, Y, Johnson, T, Zhang, F, Deisseroth, K, and Tracey, WD (2007). Nociceptive neurons protect Drosophila larvae from parasitoid wasps. Curr Biol 17, 2105–2116.

Jiang, N et al. (2019). A conserved morphogenetic mechanism for epidermal ensheathment of nociceptive sensory neurites. Elife 8.

Khuong, TM, Wang, Q-P, Manion, J, Oyston, LJ, Lau, M-T, Towler, H, Lin, YQ, and Neely, GG (2019). Nerve injury drives a heightened state of vigilance and neuropathic sensitization in Drosophila. Sci Adv 5, eaaw4099.

Kim, ME, Shrestha, BR, Blazeski, R, Mason, CA, and Grueber, WB (2012a). Integrins
704 establish dendrite-substrate relationships that promote dendritic self-avoidance and patterning in drosophila sensory neurons. Neuron 73, 79–91.

706 Kim, SE, Coste, B, Chadha, A, Cook, B, and Patapoutian, A (2012b). The role of Drosophila Piezo in mechanical nociception. Nature 483, 209–212.

708 Kim, T-J et al. (2015). Distinct mechanisms regulating mechanical force-induced Ca^{2+} signals at the plasma membrane and the ER in human MSCs. Elife 4, e04876.

710 Klapoetke, NC et al. (2014). Independent optical excitation of distinct neural populations. Nature Methods 11, 338–346.

712 Koenig, JH, Saito, K, and Ikeda, K (1983). Reversible control of synaptic transmission in a single gene mutant of Drosophila melanogaster. J Cell Biol 96, 1517–1522.

714 Koizumi, S, Fujishita, K, Inoue, K, Shigemoto-Mogami, Y, Tsuda, M, and Inoue, K (2004). Ca2+ waves in keratinocytes are transmitted to sensory neurons: the
716 involvement of extracellular ATP and P2Y2 receptor activation. Biochem J 380, 329–338.

718 Liu, X, Wang, H, Jiang, Y, Zheng, Q, Petrus, M, Zhang, M, Zheng, S, Schmedt, C, Dong, X, and Xiao, B (2019). STIM1 thermosensitivity defines the optimal preference
720 temperature for warm sensation in mice. Cell Res 29, 95–109.

Lopez-Bellido, R, Puig, S, Huang, PJ, Tsai, C-R, Turner, HN, Galko, MJ, and Gutstein,
722 HB (2019). Growth Factor Signaling Regulates Mechanical Nociception in Flies and Vertebrates. J Neurosci 39, 6012–6030.

724 Luik, RM, Wang, B, Prakriya, M, Wu, MM, and Lewis, RS (2008). Oligomerization of STIM1 couples ER calcium depletion to CRAC channel activation. Nature 454, 538–
726 542.

Maksimovic, S et al. (2014). Epidermal Merkel cells are mechanosensory cells that tune
728 mammalian touch receptors. Nature 509, 617–621.

Mandadi, S, Sokabe, T, Shibasaki, K, Katanosaka, K, Mizuno, A, Moqrich, A,
730 Patapoutian, A, Fukumi-Tominaga, T, Mizumura, K, and Tominaga, M (2009). TRPV3 in keratinocytes transmits temperature information to sensory neurons via ATP. Pflugers
732 Arch 458, 1093–1102.

Maneshi, MM et al. (2020). Orai1 Channels Are Essential for Amplification of
734 Glutamate-Evoked Ca2+ Signals in Dendritic Spines to Regulate Working and Associative Memory. Cell Rep 33, 108464.

736 Masuda, J, Tsuda, M, Tozaki-Saitoh, H, and Inoue, K (2009). Intrathecal delivery of PDGF produces tactile allodynia through its receptors in spinal microglia. Mol Pain 5,
738 23.

Mauthner, SE, Hwang, RY, Lewis, AH, Xiao, Q, Tsubouchi, A, Wang, Y, Honjo, K,
740 Skene, JHP, Grandl, J, and Tracey, WD (2014). Balboa binds to pickpocket in vivo and is required for mechanical nociception in Drosophila larvae. Curr Biol 24, 2920–2925.

742 Mederos y Schnitzler, M, Storch, U, Meibers, S, Nurwakagari, P, Breit, A, Essin, K, Gollasch, M, and Gudermann, T (2008). Gq-coupled receptors as mechanosensors
744 mediating myogenic vasoconstriction. EMBO J 27, 3092–3103.

Moehring, F, Cowie, AM, Menzel, AD, Weyer, AD, Grzybowski, M, Arzua, T, Geurts,
746 AM, Palygin, O, and Stucky, CL (2018). Keratinocytes mediate innocuous and noxious touch via ATP-P2X4 signaling. Elife 7.

748 Mohammad, F, Stewart, JC, Ott, S, Chlebikova, K, Chua, JY, Koh, T-W, Ho, J, and Claridge-Chang, A (2017). Optogenetic inhibition of behavior with anion
750 channelrhodopsins. Nat Methods 14, 271–274.

Moqrich, A, Hwang, SW, Earley, TJ, Petrus, MJ, Murray, AN, Spencer, KSR, Andahazy,
752 M, Story, GM, and Patapoutian, A (2005). Impaired thermosensation in mice lacking TRPV3, a heat and camphor sensor in the skin. Science 307, 1468–1472.

754 Morin, X, Daneman, R, Zavortink, M, and Chia, W (2001). A protein trap strategy to detect GFP-tagged proteins expressed from their endogenous loci in Drosophila. Proc
756 Natl Acad Sci USA 98, 15050–15055.

O'Brien, GS, Rieger, S, Wang, F, Smolen, GA, Gonzalez, RE, Buchanan, J, and
758 Sagasti, A (2012). Coordinate development of skin cells and cutaneous sensory axons in zebrafish. J Comp Neurol 520, 816–831.

760 Ohyama, T et al. (2015). A multilevel multimodal circuit enhances action selection in Drosophila. Nature 520, 633–639.

762 Picelli, S, Faridani, OR, Björklund, AK, Winberg, G, Sagasser, S, and Sandberg, R (2014). Full-length RNA-seq from single cells using Smart-seq2. Nat Protoc 9, 171–181.

764 Pores-Fernando, AT, and Zweifach, A (2009). Calcium influx and signaling in cytotoxic T-lymphocyte lytic granule exocytosis. Immunol Rev 231, 160–173.

766 Puig, S, Donica, CL, and Gutstein, HB (2020). EGFR Signaling Causes Morphine Tolerance and Mechanical Sensitization in Rats. ENeuro 7, ENEURO.0460-18.2020.

768 Ramesh, G et al. (2021). A short isoform of STIM1 confers frequency-dependent synaptic enhancement. Cell Rep 34, 108844.

770 Ranade, SS et al. (2014). Piezo2 is the major transducer of mechanical forces for touch sensation in mice. Nature 516, 121–125.

772 Sadler, KE, Moehring, F, and Stucky, CL (2020). Keratinocytes contribute to normal cold and heat sensation. Elife 9, e58625.

774 Schneider, CA, Rasband, WS, and Eliceiri, KW (2012). NIH Image to ImageJ: 25 years of image analysis. Nat Methods 9, 671–675.

776 Sweeney, ST, Broadie, K, Keane, J, Niemann, H, and O'Kane, CJ (1995). Targeted expression of tetanus toxin light chain in Drosophila specifically eliminates synaptic
778 transmission and causes behavioral defects. Neuron 14, 341–351.

Tsutsumi, M, Inoue, K, Denda, S, Ikeyama, K, Goto, M, and Denda, M (2009).
780 Mechanical-stimulation-evoked calcium waves in proliferating and differentiated human keratinocytes. Cell Tissue Res 338, 99–106.

782 Turner, HN et al. (2016). The TRP Channels Pkd2, NompC, and Trpm Act in Cold-Sensing Neurons to Mediate Unique Aversive Behaviors to Noxious Cold in Drosophila.
784 Curr Biol 26, 3116–3128.

Venturini, V et al. (2020). The nucleus measures shape changes for cellular
786 proprioception to control dynamic cell behavior. Science 370, eaba2644.

Williams, CR, Baccarella, A, Parrish, JZ, and Kim, CC (2016). Trimming of sequence
788 reads alters RNA-Seq gene expression estimates. BMC Bioinformatics 17, 103.

Wilson, SR, Thé, L, Batia, LM, Beattie, K, Katibah, GE, McClain, SP, Pellegrino, M,
790 Estandian, DM, and Bautista, DM (2013). The epithelial cell-derived atopic dermatitis cytokine TSLP activates neurons to induce itch. Cell 155, 285–295.

792 Woo, S-H et al. (2014). Piezo2 is required for Merkel-cell mechanotransduction. Nature 509, 622–626.

794 Xiang, Y, Yuan, Q, Vogt, N, Looger, LL, Jan, LY, and Jan, YN (2010). Light-avoidance-mediating photoreceptors tile the Drosophila larval body wall. Nature 468, 921–926.

796 Xu, J et al. (2018). GPR68 Senses Flow and Is Essential for Vascular Physiology. Cell 173, 762-775.e16.

798 Yamamoto, M, Ueda, R, Takahashi, K, Saigo, K, and Uemura, T (2006). Control of axonal sprouting and dendrite branching by the Nrg-Ank complex at the neuron-glia
800 interface. Curr Biol 16, 1678–1683.

Yin, C, Peterman, E, Rasmussen, JP, and Parrish, JZ (2021). Transparent Touch:
802 Insights From Model Systems on Epidermal Control of Somatosensory Innervation. Front Cell Neurosci 15, 680345.

804 Zhang, W, Yan, Z, Jan, LY, and Jan, YN (2013). Sound response mediated by the TRP channels NOMPC, NANCHUNG, and INACTIVE in chordotonal organs of Drosophila
806 larvae. Proc Natl Acad Sci USA 110, 13612–13617.

Zimmermann, G, Wang, L-P, Vaughan, AG, Manoli, DS, Zhang, F, Deisseroth, K,
808 Baker, BS, and Scott, MP (2009). Manipulation of an innate escape response in Drosophila: photoexcitation of acj6 neurons induces the escape response. PLoS One 4,
810 e5100.

812

Figure Legends

814

Figure 1. Stimulation of epidermal cells elicits nociceptive behaviors. (A) Fraction
816 of larvae that exhibited optogenetic-induced rolling (roll probability) using the indicated GAL4 lines to drive *UAS-CsChrimson* expression. All experimental genotypes, except
818 for larvae expressing *UAS-CsChrimson* in C4da neurons, included *elav-GAL80* to suppress neuronal GAL4 activity. Genotypes: *GAL4, UAS-CsChrimson, elav-GAL80/+*.
820 (B) Roll probability of larvae following optogenetic stimulation using the indicated GAL4 lines in combination with *elav-GAL80* (or *tsh-GAL80* + *cha-GAL80* in the case of *A58-*
822 *GAL4*) to drive *UAS-CsChrimson* expression in epidermal cells. All epidermal drivers except for *sr-GAL4*, which is expressed in apodemes but no other epidermal cells,
824 elicited rolling responses. Genotypes: *GAL4, UAS-CsChrimson, elav-GAL80/+*. (C) Roll probability of larvae following thermogenetic stimulation using the indicated GAL4 line to
826 express the warmth (35°C) -activated *UAS-TrpA1*. The number of rolling larvae (out of 50) is indicated for each group. Genotypes: *GAL4, UAS-TrpA1, GAL80 (as indicated)/+*.
828 Control, *UAS-TrpA1/+*. Asterisk (*) indicates $p<0.05$, Sample sizes are indicated in each panel. See Table 1 for details of statistical analsyes.

830

Figure 1 – figure supplement 1. Related to Figure 1A. Detailed behavior analyses of
832 larvae following optogenetic stimulation using the indicated GAL4 lines to express *UAS-CsChrimson*. (A-G) Behavior ethograms show behaviors of individual larvae (rows) prior
834 to, during, and after application of the light stimulus (indicated by the blue bar above the ethogram). (H) Fraction of larvae exhibiting indicated behaviors and (I) duration of
836 indicated behaviors during light stimulus.

838 **Figure 1 – figure supplement 2**. Related to Figure 1A. Expression patterns of body wall *GAL4* drivers. Maximum intensity projections of tiled confocal stacks show larval
840 expression of membrane-targeted RFP (*UAS-mCD2-Cherry*) by the indicated drivers in larvae additionally expressing the C4da neuron-specific marker *ppk-CD8-GFP*. Scale

842 bars, 500 μm. Genotypes: *ppk-mCD8-GFP/+; UAS-mCD2-Cherry/+; GAL4/+*

844 **Figure 1 – figure supplement 3**. Related to Figures 1A and 1C. Expression analysis of the pan-epidermal *R38F11-GAL4* driver. Maximum intensity projections of confocal
846 stacks show larval expression of a red fluorescent protein (*UAS-tdTomato*) under control of the indicated epidermal drivers in larvae additionally expressing *Nrg167-GFP*,
848 an exon trap line that labels epidermal and glial membranes (Morin *et al.*, 2001; Yamamoto *et al.*, 2006). (A-C) Peripheral expression patterns of *R38F11-GAL4*. Larvae
850 are oriented dorsal-up. (A) Low-magnification view showing stereotyped expression in dorsal epidermis across multiple larval segments. *R38F11-GAL4* is likewise expressed
852 throughout the ventral and lateral epidermis. Compared to other epidermal drivers (see Fig. 1S5), *R38F11-GAL4* exhibited more uniform expression from segment to segment
854 and among epidermal subpopulations within a given segment. (B) *R38F11-GAL4* expression in dorsal epidermis of a single abdominal segment, A2. (C) High-resolution
856 images of the larval skin territory containing dorsal cluster da neurons, which include the nociceptive neuron ddaC (outlined by dashed lines), mechanosensory neuron ddaF,
858 and proprioceptive neurons ddaD/E. Note that although *R38F11-GAL4* is expressed in epidermal cells, expression is undetectable in da neurons. The *R38F11-GAL4*
860 expression domain likewise excludes all other larval sensory neurons. (D) *R38F11-GAL4* expression in the larval CNS. *R38F11-GAL4* is expressed in a single motor
862 neuron in each segment of the ventral ganglion, ~10 VNC interneurons, and ~50 additional neurons in each brain hemisphere. (E-H) GAL80-mediated refinement of
864 *R38F11-GAL4* expression. (E) *Tsh-GAL80* induced variegation in epidermal *R38F11-GAL4* expression and (F) suppressed VNC expression while expanding brain
866 expression domains of *R38F11-GAL4*. (G) *Elav-GAL80* likewise induced epidermal variegation in *R38F11-GAL4* expression but (H) completely attenuated CNS expression.
868 Dashed lines in (F, H) outline the larval brain and ventral ganglion. Genotypes: (A-D) Nrg^{G00305}*/+; UAS-tdTomato/+;* $GAL4^{GMR38F11}$*/+*, (E-F) Nrg^{G00305}*/+; UAS-tdTomato/tsh-*
870 *GAL80;* $GAL4^{GMR38F11}$*/+*, (G-H) Nrg^{G00305}*/+; UAS-tdTomato/+;* $GAL4^{GMR38F11}$*/elav-GAL80*.

872

Figure 1 – figure supplement 4. Related to Figure 1B.

874 (A-B) Behaivior ethograms of larvae following pan-epidermal stimulation (denoted with a red bar) mediated by *A58-GAL4*. (C) Fraction of larvae exhibiting indicated behaviors

876 and (I) duration of indicated behaviors during optogenetic stimulation. (Genotype: *A58-GAL4, UAS-CsChrimson, tsh-GAL80, cha-GAL80/+*). (E-K) Behavioral ethograms of

878 larvae following optogenetic stimulation (denoted with a blue bar) with a panel of epidermal GAL4 drivers. (L) Fraction of larvae exhibiting indicated behaviors and (M)

880 duration of indicated behaviors during light stimulus. Genotype: *GAL4, UAS-CsChrimson, elav-GAL80/+*.

882

Figure 1 – figure supplement 5. Related to Figure 1B. Expression patterns of

884 epidermal GAL4 drivers in the larval body wall and CNS. Maximum intensity projections of confocal stacks show larval expression of a red fluorescent protein (*UAS-tdTomato*)

886 under control of the indicated epidermal drivers in larvae additionally expressing *Nrg167-GFP*, an exon trap line that labels epidermal and glial membranes (Morin *et al.*,

888 2001; Yamamoto *et al.*, 2006). White brackets mark the location of nociceptive C4da neuron cell bodies. Except for *A58-GAL4*, epidermal drivers used in this study exhibit

890 sparse nervous system expression. Scale bars, 200 μm. Genotypes: Nrg^{G00305}*/+; UAS-tdTomato/+; GAL4/+*

892

Figure 2. Stimulation of epidermal cells evokes multimodal behavioral responses.

894 (A) Larval behaviors were scored for 10 sec before, during, and after optogenetic stimulation. (B-E) Fraction of larvae exhibiting indicated behaviors over time in one

896 second bins expressing CsChrimson in (B) epidermal cells, (C) C4da neurons, (D) C3da neurons, and (E) Cho neurons in the presence and absence of all-trans retinal (ATR).

898 Red line indicates the presence of light stimulation. (F) The latency to the first roll of the larvae that rolled from *Epi>Chrimson* ATR+ and *C4da>Chrimson* ATR+ treatment

900 groups (n = 14, 17, respectively). (G) The duration of indicated behaviors of the larvae that displayed those behaviors during optogenetic stimulation. (H) The fraction of larvae

902 that exhibited indicated behaviors following removal of the light stimulus of all larvae from panels (B-E). Genotypes: *GAL4, UAS-CsChrimson/+*.

904

Figure 2 – figure supplement 1. (A-D) Behavior ethograms depict behaviors of
906 individual larvae displayed in one second bins over the entire time course. (E) Fraction of larvae exhibiting indicated behaviors during light stimulus. (F) Latency to the first
908 bend, hunch, back and freeze behaviors following optogenetic stimulation. Genotypes: *GAL4, UAS-CsChrimson/+*.

910

Figure 3. (A) Optogentic activation of CsChrimson-expressing epidermal cells in the
912 body wall triggers calcium transients in the axon terminal of GCaMP6s-expressing nociceptive SSNs. Images show responses from one representative animal. Plots depict
914 mean GCaMP6s fluorescence intensity of the axon terminals of (B) C4da, (C) C3da, and (D) Cho neurons following optogenetic activation (light stimulus, yellow box) of
916 epidermal cells over time. Solid lines depict mean GCaMP6s fluorescence across replicates (n=15 larval fillet preparations), shading indicates SEM, red traces are ATR+
918 and blue, ATR-. (E) The fraction of larvae exhibiting indicated behaviors during optogenetic epidermal stimulation in combination with SSN silencing via Tetanus Toxin
920 (TnT) expression. (F) The duration of the behavioral responses during optogenetic epidermal stimulation with neuronal TnT expression. Genotypes: (A-C) *AOP-GCaMP6s,*
922 *UAS-CsChrimson; R38F11-GAL4/+* together with the following LexA drivers: *R27H06-LexA* (C4da neurons), *NompC-LexA* (C3da neurons); (D) *UAS-GCaMP6s, AOP-*
924 *CsChrimson, R61D08-GAL4/R38F11-LexA*; (E-F) *R38F11-GAL4, UAS-CsChrimson, AOP-LexA-TnT/+* (*Epi>CsChrimson*); *R38F11-GAL4, UAS-CsChrimson, AOP-LexA-*
926 *TnT/ppk-LexA* (*Epi>CsChrimson + C4da>TnT*); *R38F11-GAL4, UAS-CsChrimson, AOP-LexA-TnT/NompC-LexA* (*Epi>CsChrimson + C3da>TnT*).

928

Figure 3 – figure supplement 1. Related to Figure 3A-3D. GCaMP6s responses in
930 axon terminals of (B) C4da, (C) C3da, and (D) Cho neurons following optogenetic activation (light stimulus, yellow box) of epidermal cells over time. Each trace represents

932 the GCaMP6s fluorescence of an individual larval fillets. Red traces are ATR+ and blue, ATR-.

934

Figure 3 – figure supplement 2. Related to Figure 3E-3F. (A-C) Behavior ethograms
936 (left) and fraction of larvae (right) exhibiting indicated behaviors to optogenetic epidermal stimulation in combination with (A) an *AOP-TNT* transgene (control lacking
938 LexA driver), (B) C4da neuron silencing via Tetanus Toxin (TnT), and (C) C3da neuron silencing via TnT. (D) Fraction of larvae exhibiting each behavior and (E) the duration of
940 behavior responses after removal of the light stimulus. Genotypes are indicated in (A-C).

942

Figure 4. Epidermal stimulation augments nociceptive responses. (A) Mean GCaMP6s
944 responses (F/F_0) in C4da axons during optogenetic stimulation (yellow box) of C4da neurons alone (green) or of C4da neurons and epidermal cells (magenta), shading
946 indicates SEM. (B) Simultaneous epidermal stimulation increased the peak calcium response (F_{max}/F_0), (C) total calcium influx (area under the curve), and (D) duration of
948 C4da neuron calcium responses compared to stimulation of C4da neurons alone. Genotypes: *ppk-LexA, AOP-GCAMP6s/+; R27H06-GAL4/UAS-CsChrimson* (C4da) and
950 *ppk-LexA, AOP-GCAMP6s/+; R27H06-GAL4/R38F11-GAL4, UAS-CsChrimson* (C4da+epi). (E-J) Characterization of the behavioral responses to low-intensity
952 optogenetic stimulation of C4da neurons, epidermal cells, or simulteanous C4da neurons and epidermal cells. (E) Cumulative and (F) total roll probability during
954 optogenetic stimulation (indicated by the red bar). n = 33 (*C4da>CsChrimson*), 30 (*Epi>CsChrimson*), and 31 (*C4da + Epi>CsChrimson*) larvae. (G, H) Number and
956 frequency distribution of rolls, (I) latency to the first roll observed for larvae of the indicated genotypes, and (J) the duration of the indicated behaviors during light
958 stimulus. Genotypes: *UAS-CsChrimson/+; R27H06-GAL4/+* (C4da), *UAS-CsChrimson/+; R38F11-GAL4/+* (Epidermis), *UAS-CsChrimson/+; R27H06-*
960 *GAL4/R38F11-GAL4* (C4da+Epidermis). (K) Roll probability of larvae to a 20 mN or 50 mN von Frey mechanical stimulus and epidermal optogenetic activation (a light

962 stimulus, 30mW/cm^2 that was insufficient on its own to induce nocifensive rolling).
Larvae were reared in the presence or absence of ATR, as indicated. Genotypes: *UAS-*
964 *CsChrimson/+; R38F11-GAL4/+*. (L-N) Prior epidermal but not nociceptor stimulus
potentiates mechanical nociceptive responses. (L) Roll probability of control larvae
966 (*UAS-TrpA1/+*) or larvae expressing TrpA1 in the epidermis (*Epi-GAL4: R38F11-GAL4)*
or C4da neurons (*UAS-TrpA1/+*; *C4da-GAL4 #1: R27H06-GAL4, UAS-TrpA1/+*; *C4da-*
968 *GAL4 #2: ppk-GAL4, UAS-TrpA1/+*), or control larvae (*no GAL4: UAS-TrpA1/+*;) in
response to 40 mN mechanical stimulus 10 sec following 10 sec of a thermal stimulus
970 (25º or 32º C). To control for effects of genetic background, we confirmed that each of
the experimental genotypes exhibited mechanically induced nociceptive sensitization
972 (Fig. 4S1C). (M) Roll probability of control larvae (*UAS-TrpA1/+*) or larvae expressing
TrpA1 in the epidermis (*Epi>TrpA1*: *R38F11-GAL4, UAS-TrpA1/+*) in response to a 40
974 mN mechanical stimulus delivered at the indicated time interval following a 32º C
thermal stimulus. (N) Nociceptive enhancement (difference in the roll probablity to the
976 first and second stimulus) is plotted against the recovery duration and results were fit to
an exponential curve to derive the decay time constant. The red line indicates
978 nociceptive enhancement of a mechanical stimulus by a prior epidermal thermogenetic
stimulus; the black line indicates nociceptive enhancement by a prior mechanical
980 stimulus.

982 **Figure 4 – figure supplement 1.** (A) GCaMP6s responses (F/F_0) of individual
replicates during optogenetic stimulation (yellow box) of C4da neurons alone (green) or
984 C4da neurons and epidermal cells (magenta), yellow box indicates presence of light
stimulus. Genotypes: *ppk-LexA, AOP-GCAMP6s/+; R27H06-GAL4/UAS-CsChrimson*
986 (C4da) and *ppk-LexA, AOP-GCAMP6s/+; R27H06-GAL4/R38F11-GAL4, UAS-*
CsChrimson (C4da+epi). (B) Roll probability of larvae in response to two successive 40
988 mN mechanical stimuli spaced by the indicated amount of time (recovery duration).
Genotype: *R38F11-GAL4/+*. (C) Roll probability of larvae expressing *UAS-TrpA1* in
990 nociceptors exhibited levels of mechanically induced nociceptive potentiation

comparable to other experimental genotypes used in the study (control*: UAS-TrpA1/+*;
992 epidermis*: R38F11-GAL4, UAS-TrpA1/+*; nociceptors*: R27H06-GAL4, UAS-TrpA1/+*).

994 **Figure 5.** Epidermal cells are intrinsically mechanosensitive. (A) Schematic of preparation to measure radial stretch evoked calcium responses of dissociated
996 epidermal cells. (B) Representative calcium responses of a dissociated epidermal cell to 0.5 and 1% radial stretch. (C) Dose response curve displaying the fraction of epidermal
998 cells activated by increasing magnitudes of stretch. Red trace displays the mean ± SEM across six independent dissociated cell preparations, obtained from a minimum of 6
1000 larvae. Gray traces display fraction responding in each dissociated cell preparation replicate. (D) Subsets of epidermal cells display varying stretch thresholds, n = 6
1002 dissociated cell preparations, for a total of 654 epidermal cells. (E) Representative mechanically induced epidermal calcium responses in the larval body wall. Images
1004 show GCaMP6s fluorescence intensity 100 msec prior to (i) and 20 sec following (ii) a 25 μm membrane displacement (poke). (F) Distribution of the peak calcium response
1006 (F_{max}/F_0) to a 25 μm membrane displacement (poke) of 24 cells from 24 independent larval fillets. Cells were classified as responders (>10% increase in normalized
1008 GCaMP6s fluorescence). (G) Mean calcium responses (F/F_0) of poke responders and non-responders (n = 12 cells each). Solid lines depict mean normalized GCaMP6s
1010 fluorescence and shading indicates SEM. Genotype: *R38F11-GAL4, UAS-GCaMP6s*.

1012 **Figure 5 – figure supplement 1.** Subsets of epidermal cells display calcium responses to diverse mechanical stimuli. Representative calcium traces of epidermal cells that
1014 respond to: (A) laminar flow via perfusion, (B) laminar flow and osmotic stretch, (C) 15% hypo-osmotic stretch, and (D) 30% hypo-osmotic stretch, or (E) do not respond to either
1016 flow or stretch. (F) Proportion of epidermal cells that are sensitive to mechanical stimuli. n = three distinct cell preparations, 6 larvae per preparation, for a total of 177 cells. (G)
1018 Related to Figure 5G. GCaMP6s responses (F/F_0) of individual epidermal cells to a 25 μm membrane displacement. Genotype: *R38F11-GAL4, UAS-GCaMP6s*.

1020 **Figure 6**. CRAC channels are required for epidermal mechanosensory responses and epidermal nociceptive potentiation. (A) RNAi screen for epidermal ion channels required
1022 for mechanically induced nociceptive potentiation. Bars depict nociceptive potentiation index (difference in the larval roll probability to the first and second mechanical stimuli
1024 divided by roll probability to the first mechanical stimulus). Candidate channels were chosen for further analysis if they had a a z-score greater than 2 (absolute value). (B)
1026 The CRAC channels Orai and Stim are required in epidermal cells for mechanically evoked nociceptive potentiation. Roll probability of larvae of the indicated genotypes
1028 (Control RNAi, *R38F11-GAL4, UAS-RFP-RNAi/+*; *Stim* RNAi, *R38F11-GAL4, UAS-Stim-RNAi/+*; *Orai* RNAi, *R38F11-GAL4, UAS-Orai-RNAi/+*) to a 40 mN mechanical
1030 stimulus followed by a second 40mN mechanical stimulus 10 sec later. (C) *Drosophila* epidermal cells display classical store-operated calcium entry (SOCE). Treatment with
1032 the drug thapsigargin (TG) in the absence of extracellular calcium promoted depletion of intracellular calcium stores and calcium influx, following extracellular calcium re-
1034 addition. (D-E) The fraction of stretch-sensitive epidermal cells is significantly decreased in cells isolated from larvae expressing *Stim* RNAi, or *Orai* RNAi, as compared to
1036 control RNAi. (F-G) The Orai blocker, lanthanum chloride (500 nM) or the depletion of intracellular stores by thapsigargin (1 μM) reduces the fraction of stretch-sensitive
1038 epidermal cells. (H) Stretch stimuli evoke dose-dependent calcium signals in the human keratinocyte HaCaT cell line. (I) Representative stretch-evoked SOCE calcium response
1040 in HaCaT cells. Stretch induces calcium release from stores in the absence of extracellular calcium and a greater calcium influx in the presence of extracellular
1042 calcium. (J) Epidermal hyperpolarization enhances mechanical nocifensive responses. Roll probability of larvae expressing GtACR in epidermal cells (*R38F11-GAL4, UAS-*
1044 *GtACR/+*) or control larvae (*R38F11-GAL4/+*) to a single 70 mN mechanical stimulus. (K) Epidermal *Stim* overexpression enhances mechanical nocifensive responses. Roll
1046 probability of *Stim*-overexpressing larvae (*R38F11-GAL4, UAS-Stim/+*) and control larvae (*R38F11-GAL4/+*) to two successive 40 mN mechanical stimuli delivered 10 sec
1048 apart. (L) Epidermal potentiation of mechanical nociceptive responses requires exocytosis. Roll probability of control larvae (*UAS-shi^{ts}/+*) or larvae expressing

1050 temperature-sensitive dominant-negative shibire in epidermal cells (*R38F11-GAL4, UAS-shi^{ts}/+*) in response to two successive mechanical stimuli that followed conditioning
1052 at the permissive (25° C) or non-permissive (30° C) temperature. (M) Model of epidermal-neuronal signaling. Mechanically evoked Stim/Orai calcium signaling in
1054 epidermal cells drives calcium influx and vesicle release that drives nociceptor activation and mechanical sensitization via activation of C4da nociceptors.
1056

Figure 6 – figure supplement 1. Related to Figure 6A. Ion channel expression in
1058 epidermal cells. Five populations of *UAS-GFP*-expressing epidermal cells were selected for RNA-seq analysis. GFP-positive epidermal cells were dissociated into single cell
1060 suspensions, manually picked, and subjected to RNA-Seq analysis. Plots depict expression levels (mean +/- standard deviation) of the indicated ion channels
1062 ($\log_2$(TPM+1)) from n > 6 independent libraries for each sample type.
(A) Expression in epidermal cells collected from *R38F11-GAL4* which labels all
1064 epidermal cells. (B) Anatomically defined subsets of epidermal cells were profiled by removing posterior segments from *R38F11-GAL4, UAS-GFP* larvae (*R38F11-GAL4*
1066 head and thorax) or (C) dissecting the ventral epidermis (*R38F11-GAL4* ventral epidermis). (D) Expression in the dorsal epidermis (*ush-GAL4*) and or (E) bands of
1068 epidermal cells (*R51F10-GAL4).*

1070 **Figure 6 – figure supplement 2**. (A-B) Epidermal knockdown of ion channels affects larval mechanical nociceptive responses. Roll probability in response to the first and
1072 second mechanical stimulus for larvae expressing RNAi transgenes to (A) *Orai* or *attP40* RNAi control transgene and (B) *Task6* or *attP2* RNAi control transgene. (C)
1074 Epidermal cell SOCE is attenuated by pre-treatment with the Orai blocker, lanthanum chloride (100 nM). (D) Representative SOCE after treatment with TG (1 µM) in
1076 epidermal cells isolated from larvae treated with control RNAi, *Stim* RNAi (red), or *Orai* RNAi, (blue). (E) Peak calcium response following SOCE in epidermal cells isolated
1078 from larvae treated with control RNAi, *Stim* RNAi (red), or *Orai* RNAi, (blue). (F) *Stim* RNAi decreases calcium store content of epidermal cells. Calcium store content was

1080 measured as the area under the curve of the cytosolic calcium response to TG (1 μM) in the absence of extracellular calcium.

Details of Statistical Analysis

Figure 1C: Fisher's exact test with BH correction

UAS-TRPA1 groups (25 C vs 32 C)	p-value	q-value	Significance (q<0.05)
Control (no *GAL4* driver)	0.2424	2.424000e-01	F
R27H06-GAL4	2.2e-16	3.666667e-16	T
R38F11-GAL4	2.2e-16	3.666667e-16	T
R38F11-GAL4 + elav-GAL80	2.2e-16	3.666667e-16	T
R38F11-GAL4 + tshGAL80	4.111e-15	5.138750e-15	T

Figure 1S4C: Fisher's exact test

	p-value	Significance
rolling	0.0002928	T
c-bend	2.035e-10	T
backing	0.0008424	T
hunch	0.004233	T
freeze	0.002342	T

Figure 1S5D: Wilcoxon rank sum test

	p-value	Significance
rolling	Cannot compare	
c-bend	0.8907	F
backing	0.00127	T
hunch	Cannot compare	
freeze	Cannot compare	

Figure 2F: Wilcoxon Rank-Sum test

	p-value	Significance
C4da vs Epi	0.0067	T

Figure 2G: Kruskal-Wallis test followed by Wilcoxon rank sum test with BH correction

	p-value	q-value	Significance (q<0.05)
Kruskal-Wallis test, rolling	N/A (only epi + C4da have values)		
rolling C4da vs Epi	0.03124		T
Kruskal-Wallis test, c-bend	0.0001652		T
c-bend C4da vs Epi	0.001468	0.002936	T
c-bend C3da vs Epi	0.3237	0.323700	F

Figure 2H Fisher's exact test with a BH correction

	p-value	q-value	Significance (q<0.05)
rolling Epi ATR+ vs ATR-	0.04313	0.09102	F
rolling C4da ATR+ vs ATR-	0.04551	0.09102	F
rolling C3da ATR+ vs ATR-	1	1	F
rolling Cho ATR+ vs ATR	1	1	F
c-bend Epi ATR+ vs ATR-	0.4687	0.9508	F
c-bend C4da ATR+ vs ATR-	0.4754	0.9508	F
c-bend C3da ATR+ vs ATR	1	1	F
c-bend Cho ATR+ vs ATR	1	1	F
back Epi ATR+ vs ATR-	0.00000000000004556	0.00000000000018224	T
back C4da ATR+ vs ATR	1	1	F

back C3da ATR+ vs ATR	1	1	F
back Cho ATR+ vs ATR-	0.1128	0.2256	F
hunch Epi ATR+ vs ATR	1	1	F
hunch C4da ATR+ vs ATR	1	1	F
hunch C3da ATR+ vs ATR-	1	1	F
hunch Cho ATR+ vs ATR-	0.4918	1	F
freeze Epi ATR+ vs ATR-	0.00000008682	0.00000034728	T
freeze C4da ATR+ vs ATR-	0.4754	0.6338667	F
freeze C3da ATR+ vs ATR-	1	1	F
freeze Cho ATR+ vs ATR-	0.000825	0.00165	T

Figure 2S1E: Fisher's exact test with BH correction

	p-value	q-value	Significance (q<0.05)
rolling Epi ATR+ vs ATR-	3.039e-06	6.0780e-06	T
rolling C4da ATR+ vs ATR-	9.667e-08	3.8668e-07	T
rolling C3da ATR+ vs ATR-	1	1.0000e+00	F
rolling Cho ATR+ vs ATR-	1	1.0000e+00	F
c-bend Epi ATR+ vs ATR-	1.388e-11	2.776e-11	T
c-bend C4da ATR+ vs ATR-	1.265e-11	2.776e-11	T
c-bend C3da ATR+ vs ATR-	0.00192	2.560e-03	T
c-bend Cho ATR+ vs ATR-	1	1.000e+00	F
back Epi ATR+ vs ATR-	1.238e-13	4.952000e-13	T
back C4da ATR+ vs ATR-	0.6003	6.003000e-01	F
back C3da ATR+ vs ATR-	0.02597	5.194000e-02	F
back Cho ATR+ vs ATR-	0.05251	7.001333e-02	F
hunch Epi ATR+ vs ATR-	0.04313	5.750667e-02	F
hunch C4da ATR+ vs ATR-	0.4754	4.754000e-01	F
hunch C3da ATR+ vs ATR-	1.03e-06	2.060000e-06	T
hunch Cho ATR+ vs ATR-	2.571e-14	1.028400e-13	T
freeze Epi ATR+ vs ATR-	0.01869	0.0747600	F
freeze C4da ATR+ vs ATR-	0.2219	0.2958667	F
freeze C3da ATR+ vs ATR-	0.5353	0.5353000	F
freeze Cho ATR+ vs ATR-	0.05251	0.1050200	F

Figure 3E Fisher's exact test with BH correction

	p-value	q-value	Significance (q<0.05)
rolling control vs *C4da>TNT*	0.001051	0.002102	T
rolling control vs *C3da>TNT*	0.1945	0.194500	F
c-bend control vs *C4da>TNT*	1	1.00000	F
c-bend control vs *C3da>TNT*	0.05219	0.10438	F
back control vs *C4da>TNT*	0.7787	0.778700	F
back control vs *C3da>TNT*	0.005579	0.011158	T
hunch control vs *C4da>TNT*	0.02372	0.04744	T
hunch control vs *C3da>TNT*	0.1124	0.11240	F
freeze control vs *C4da>TNT*	0.3533	0.3533	F
freeze control vs *C3da>TNT*	0.1945	0.3533	F

Figure 3F Kruskal-Wallis test followed by Wilcoxon rank sum test with BH correction

	p-value	q-value	Significance (q<0.05)
Kruskal-Wallis test, rolling	0.0004424		
rolling control vs *C4da>TNT*	0.001122	0.002244	T
rolling control vs *C3da>TNT*	0.7007	0.700700	F

Kruskal-Wallis test, c-bend	0.001948		
c-bend control vs *C4da>TNT*	0.0004278	0.0008556	T
c-bend control vs *C3da>TNT*	0.433	0.4330000	F
Kruskal-Wallis test, back	0.4203		
back control vs *C4da>TNT*	N/A		
back control vs *C3da>TNT*	N/A		
hunch control vs *C4da>TNT*	No Hunch in control		
hunch control vs C3da TNT	No Hunch in control (p=0.4127 C4vsC3)		
Kruskal-Wallis test, freeze	0.3808		
freeze control vs *C4da>TNT*	N/A		
freeze control vs *C3da>TNT*	N/A		

Figure 3S2 D: Fisher's exact test with BH correction

	p-value	q-value	Significance (q<0.05)
Control vs C4da silence, roll	0.0003682	0.0007364	T
Control vs C3da silence, roll	0.3015	0.3015000	F
Control vs C4da silence, c-bend	0.1188	0.2376	F
Control vs C3da silence, c-bend	0.2949	0.2949	F
Control vs C4da silence, backward	1	1.00000	F
Control vs C3da silence, backward	0.02372	0.04744	T
Control vs C4da silence, hunch	1	1	F
Control vs C3da silence, hunch	1	1	F
Control vs C4da silence, freeze	0.1028	0.102800	F
Control vs C3da silence, freeze	0.002466	0.004932	T

Figure 3S2 E: Kruskal-Wallis test followed by Wilcoxon rank sum test

	p-value	q-value	Significance
Kruskal-Wallis test, Roll	0.02471		T
Control vs C4da silence Roll	0.01604	0.03208	T
Control vs C3da silence Roll	0.04658	0.04658	T
Kruskal-Wallis test, c-bend	0.01971		T
Control vs C4da silence c-bend	0.008927	0.017854	T
Control vs C3da silence c-bend	0.02334	0.023340	T
Control vs C4da silence back	0.2222		F
Control vs C3da silence back	N/A		
Control vs C3da silence back	N/A		
Control vs C4da silence hunch	N/A		
Control vs C3da silence hunch	N/A		
Control vs C4da silene freeze	N/A		
Control vs C3da silence freeze	N/A		

Figure 4B: Wilcoxon Rank-Sum test

	p-value	Significance
Fmax/F0 C4da vs C4da +Epi	0.0288	T

Figure 4C: Wilcoxon Rank Sum test

	p-value	q-value	Significance (q<0.05)
C4da vs C4da+Epi	0.03184		T

Figure 4D: Wilcoxon Rank-Sum test

	p-value	Significance

C4da vs C4da+Epi	0.03277	T

Figure 4F: Fisher's exact test with BH correction

	p-value	q-value	Significance (q<0.05)
C4da vs Epi	0.0003136	3.741e-04	T
C4da vs Epi+C4da	0.7541	3.741e-04	T
Epi vs Epi+C4da	0.000005162	2.997e-11	T

Figure 4G: Kruskal-Wallis test followed by Wilcoxon rank sum test with BH correction

	p-value	q-value	Significance (q<0.05)
Kruskal-Wallis test	0.000000001544		
C4da vs Epi	0.7541	0.7541	F
C4da vs Epi+C4da	0.000000000001072	0.000000000003216	T
Epi vs Epi+C4da	0.000005162	0.000007743	T

Figure 4H: Fisher's exact test with BH correction

	p-value	q-value	Significance (q<0.05)
<5 C4da vs Epi	0.1894	1.894e-01	F
<5 C4da vs C4da+Epi	3.646e-11	5.469e-11	T
<5 Epi vs C4da+Epi	2.571e-14	7.713e-14	T
5-9 C4da vs Epi	0.674	0.674	F
5-9 C4da vs C4da+Epi	0.356	0.674	F
5-9 Epi vs C4da+Epi	0.6124	0.674	F
10 -14 C4da vs Epi	0.6144	0.9216	F
10 -14 C4da vs C4da+Epi	1	1.0000	F
10 -14 Epi vs C4da+Epi	0.6124	0.9216	F
15 -19 C4da vs Epi	1	1.0000	F
15-19 C4da vs C4da+Epi	0.1896	0.2844	F
15 -19 Epi vs C4da+Epi	0.1128	0.2844	F
>20 C4da vs Epi	1	1.0000	F
>20 C4da vs C4da+Epi	5.377e-11	1.6131e-10	T
>20 Epi vs C4da+Epi	2.644e-10	3.9660e-10	T

Figure 4I: Kruskal-Wallis test followed by Wilcoxon rank sum test with BH correction

	p-value	q-value	Significance (q<0.05)
Kruskal-Wallis test	5.993e-15		
C4da vs Epi	0.0009667	9.6670e-04	T
C4da vs Epi+C4da	4.97e-15	7.4550e-15	T
Epi vs Epi+C4da	5.028e-16	1.5084e-15	T

Figure 4J: Kruskal-Wallis test followed by Wilcoxon rank sum test with BH correction

	p-value	q-value	Significance (q<0.05)
Kruskal-Wallis test, rolling	4.024e-09		T
roll C4da vs Epi	0.1937	1.9370e-01	F
roll C4da vs C4da+Epi	9.024e-12	2.7072e-11	T
roll Epi vs C4da + Epi	5.506e-05	8.2590e-05	T
Kruskal-Wallis test, c-bend	0.06175		F
c-bend C4da vs Epi	N/A		
c-bend C4da vs C4da+Epi	N/A		
c-bend Epi vs C4da +Epi	N/A		
Kruskal-Wallis test, backing	9.145e-06		T

back C4da vs Epi	9.574e-07	2.8722e-06	T
back C4da vs C4da+Epi	0.02662	2.6620e-02	T
back Epi vs C4da+Epi	0.001987	2.9805e-03	T
Kruskal-Wallis test, hunching	0.006437		T
hunch C4da vs Epi	0.2706	0.270600	F
hunch C4da vs C4da+Epi	0.001252	0.003756	T
hunch Epi vs C4da+Epi	0.1836	0.270600	F
Kruskal-Wallis test, freezing	0.4857		F
freeze C4da vs Epi	N/A		
freeze C4da vs C4da+Epi	N/A		
freeze Epi vs C4da+Epi	N/A		

Figure 4K: Fisher's exact test with a BH correction

Epi-GAL4, UAS-CsChrimson treatment groups	p-value	q-value	Significance
20 mN ATR- vs ATR+ Epi>CsChrimson	0.003234	0.0097020	T
50 mN ATR- vs ATR+ Epi>CsChrimson	0.008797	0.0131955	T
50mN ATR- vs ATR+ CsChrimson	0.7639	0.7639000	F

Figure 4L: Fisher's exact test with BH correction

	p-value	q-value	Significance (q<0.05)
No *GAL4* 25 vs 32	0.6798	0.7806000	F
Epi-GAL4 25 vs 32	0.0005454	0.0021816	T
27H06-GAL4 25 vs 32	0.7806	0.7806000	F
ppk-GAL4 25 vs 32	0.7735	0.7806000	F

Figure 4M: Fisher's exact test with BH correction

UAS-TRPA1 comparisons	p-value	q-value	Significance (q<0.05)
10sec control vs 10sec *Epi-GAL4*	0.006108	0.01018000	T
30sec control vs 30sec *Epi-GAL4*	0.001265	0.00316250	T
60sec control vs 60sec *Epi-GAL4*	0.00007129	0.00035645	T
300sec control vs 300sec *Epi-GAL4*	0.07531	0.09413750	F
600sec control vs 600sec *Epi-GAL4*	0.4351	0.43510000	F

Figure 4N: Curve fitting

	fit curve	Decay time constant
Mechano (Fig 4S1B)	f(x) = 0.4139*exp(-0.002994*x)	334.001336
Epidermal activation (Fig 4L)	f(x) = 0.47*exp(-0.002964*x)	337.3819163

Figure 4S1B: Fisher's exact test with BH correction

	p-value	q-value	Significance (q<0.05)
10sec 1st vs 2nd	0.0007546	0.0018865	T
30sec 1st vs 2nd	0.000006865	0.000034325	T
60sec 1st vs 2nd	0.008544	0.01424	T
300sec 1st vs 2nd	0.131	0.16375	F
600sec 1st vs 2nd	0.3217	0.3217	F

Figure 4S1C: Fisher's exact test with BH correction

	p-value	q-value	Significance (q<0.1)
Control 1st vs 2nd	0.006746	0.00674600	T
Epi-GAL4 1st vs 2nd	6.336e-05	0.00019008	T
Nociceptor-GAL4 1st vs 2nd	0.005186	0.00674600	T

Figure 6B Fisher's exact test with BH correction

	p-value	q-value	Significance (q<0.1)
Control 1st vs 2nd	4.94E-05	0.0002472	T
Orai RNAi 1st vs 2nd	0.1329	0.3236667	F
Stim RNAi 1st vs 2nd	0.1942	0.3236667	F
Control 1st vs *Orai* RNAi 1st	0.8788	0.6660000	F
Control 1st vs *Stim* RNAi 1st	0.5328	0.8788000	F

Figure 6E: Chi-square comparing distribution of stretch sensitive cells

	Chi-square value	DF	p-value
Control vs *Stim* RNAi	33	4	<0.0001
Control vs *Orai* RNAi	150.6	4	<0.0001
Stim RNAi vs *Orai* RNAi	3.689	4	0.4497

Figure 6G: Chi-square comparing distribution of stretch sensitive cells

	Chi-square value	DF	p-value
Control vs La3+	36.09	4	<0.0001
Control vs Store Depleted	112.1	4	<0.0001
Store Depleted vs La3+	40.69	4	<0.0001

Figure 6J: Fisher's exact test

	p-value		
control vs *GtACR*	0.03216		

Figure 6K Fisher's exact test with BH correction

	p-value	q-value	Significance (q<0.1)
Control 1st vs 2nd	0.00037	0.00148000	T
Stim OE 1st vs 2nd	0.02386	0.03181333	T
Control 1st vs *Stim OE* 1st	0.002115	0.00423000	T

Figure 6L: Fisher's exact test with BH correction

	p-value	q-value	Significance
Control 25C 1st vs Control 25C 2nd	5.425e-05	7.233333e-05	T
Control 30C 1st vs Control 30C 2nd	1.033e-06	2.066000e-06	T
Epi>shi 25C 1st vs *Epi>shi* 25C 2nd	4.912e-07	1.964800e-06	T
Epi>shi 30C 1st vs *Epi>shi* 30C 2nd	0.05076	5.076000e-02	F

Figure 6S2A Fisher's exact test with BH correction

	p-value	q-value	significance
Control Trial 1 vs Trial 2	0.002438	0.004876	T
Orai RNAi Trial 1 vs Trial 2	0.4076	0.4076	F

Figure 6S2B Fisher's exact test with BH correction

	p-value	q-value	significance
Control Trial 1 vs Trial 2	0.00157	0.003140	T
Task6 RNAi Trial 1 vs Trial 2	0.004795	0.004795	T

Figure 6S2C Wilcoxon Rank-Sum test

	p-value	significance
Control vs La^{3+} block	0.0003377	T

Figure 6S2E: Kruskal-Wallis test followed by Wilcoxon rank sum test with BH correction

	p-value	q-value	Significance (q<0.05)
Kruskal-Wallis test	0.00001332		T
Control vs *Stim* RNAi	0.0009161	0.001374150	T
Control vs *Orai* RNAi	0.000005094	0.000015282	T
Stim RNAi vs *Orai* RNAi	0.3759	0.375900000	F

Figure 6S2F: Kruskal-Wallis test followed by Wilcoxon rank sum test with BH correction

	p-value	q-value	Significance (q<0.05)
Kruskal-Wallis test	0.004105		T
Control vs *Stim* RNAi	0.001296	0.002592	T
Control vs *Orai* RNAi	0.8294	0.829400	F

Yoshino et al, Fig. 1

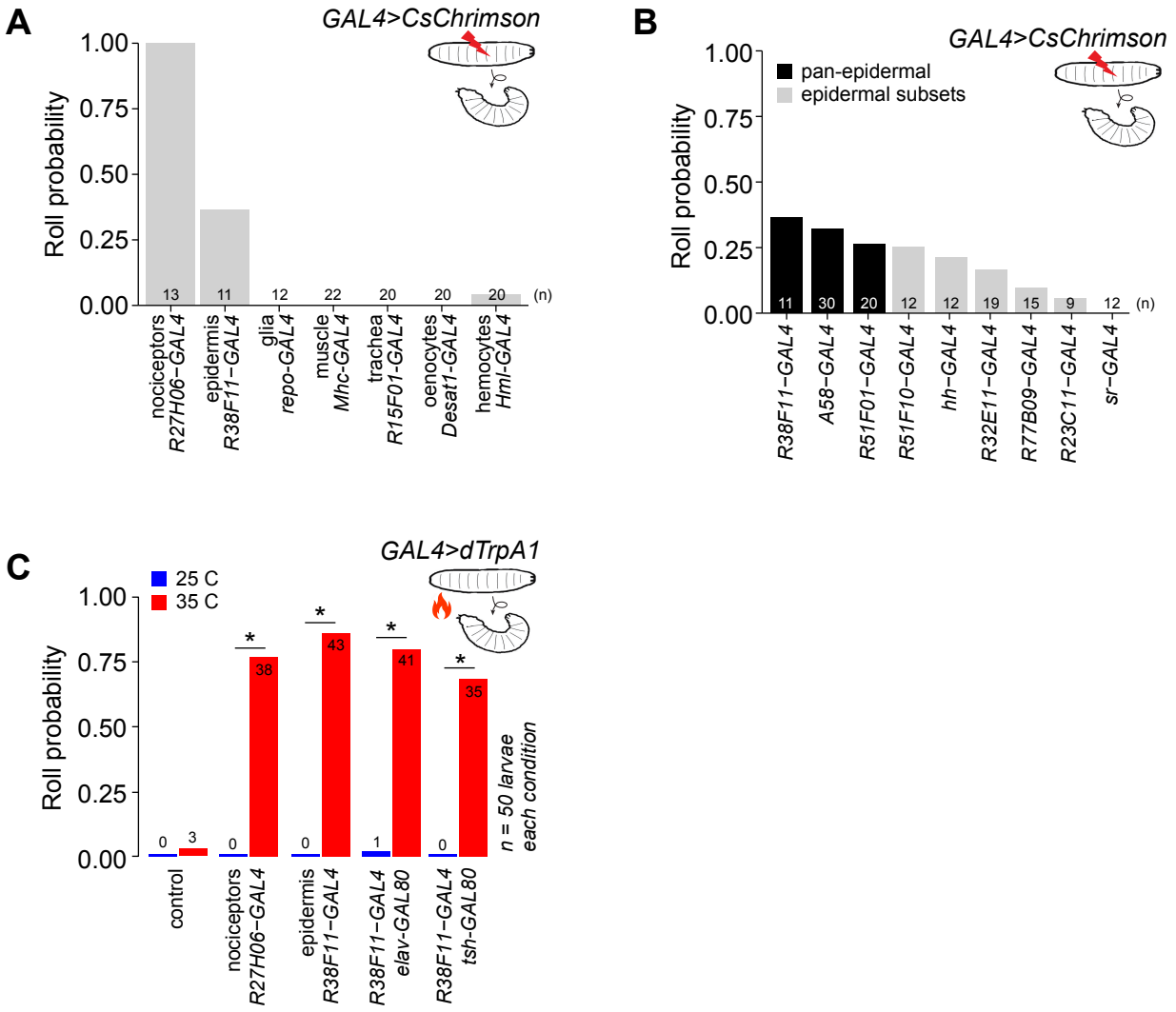

Figure 1. Stimulation of epidermal cells elicits nociceptive behaviors. (A) Fraction of larvae that exhibited optogenetic-induced rolling (roll probability) using the indicated GAL4 lines to drive *UAS-CsChrimson* expression. All experimental genotypes, except for larvae expressing *UAS-CsChrimson* in C4da neurons, included *elav-GAL80* to suppress neuronal GAL4 activity. Genotypes: *GAL4, UAS-CsChrimson, elav-GAL80/+*. (B) Roll probability of larvae following optogenetic stimulation using the indicated GAL4 lines in combination with *elav-GAL80* (or *tsh-GAL80* + *cha-GAL80* in the case of *A58-GAL4*) to drive *UAS-CsChrimson* expression in epidermal cells. All epidermal drivers except for *sr-GAL4*, which is expressed in apodemes but no other epidermal cells, elicited rolling responses. Genotypes: *GAL4, UAS-CsChrimson, elav-GAL80/+*. (C) Roll probability of larvae following thermogenetic stimulation using the indicated GAL4 line to express the warmth (35º C)-activated *UAS-TrpA1*. The number of rolling larvae (out of 50) is indicated for each group. Genotypes: *GAL4, UAS-TrpA1, GAL80* (as indicated)/+. Control, *UAS-TrpA1/+*. Asterisk (*) indicates p<0.05, Sample sizes are indicated in each panel. See Table 1 for details of statistical analsyes.

Yoshino et al, Fig. 1S1

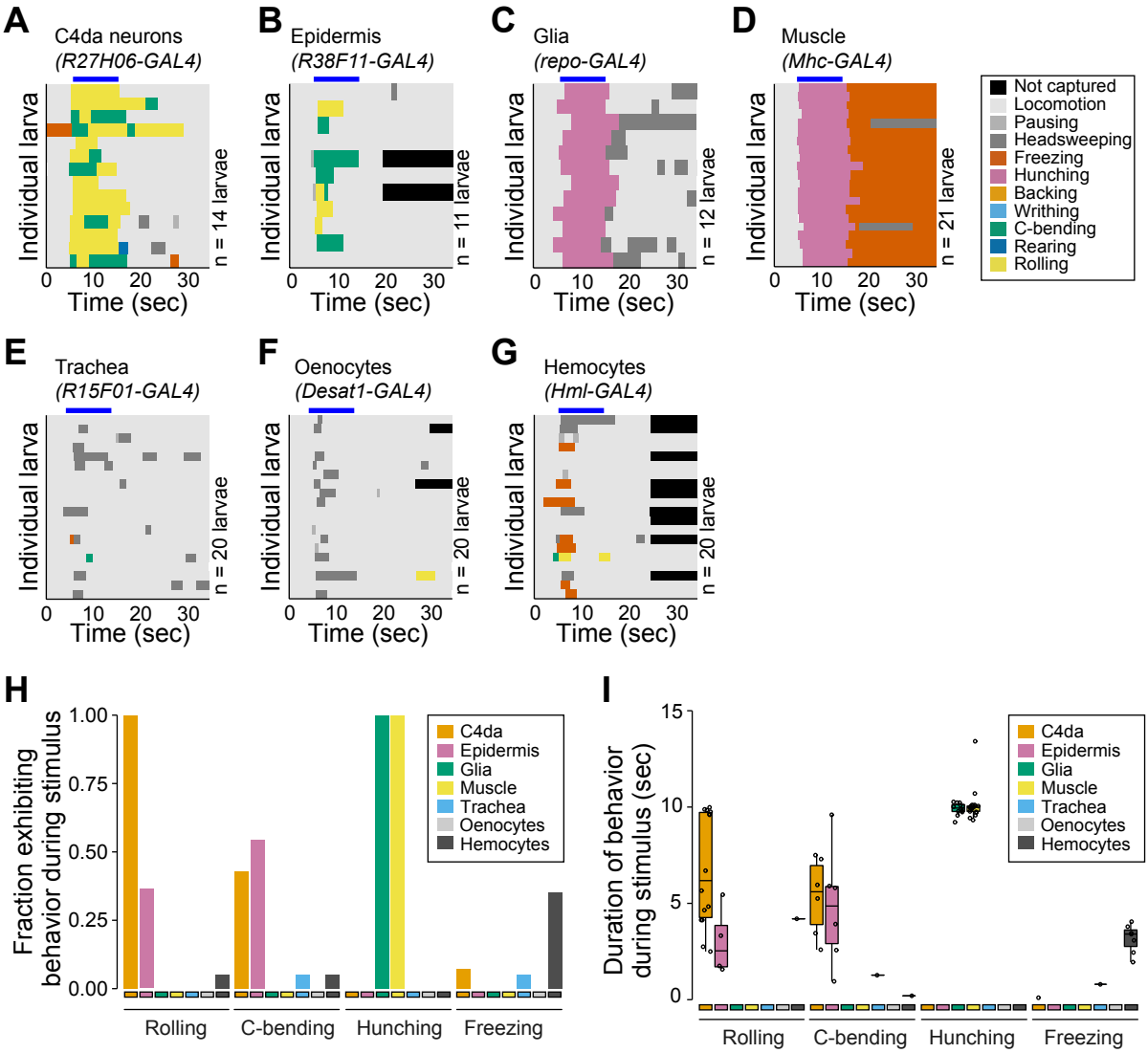

Figure 1 – figure supplement 1. Related to Figure 1A. Detailed behavior analyses of larvae following optogenetic stimulation using the indicated GAL4 lines to express *UAS-CsChrimson*. (A-G) Behavior ethograms show behaviors of individual larvae (rows) prior to, during, and after application of the light stimulus (indicated by the blue bar above the ethogram). (H) Fraction of larvae exhibiting indicated behaviors and (I) duration of indicated behaviors during light stimulus.

Yoshino et al, Fig. 1S2

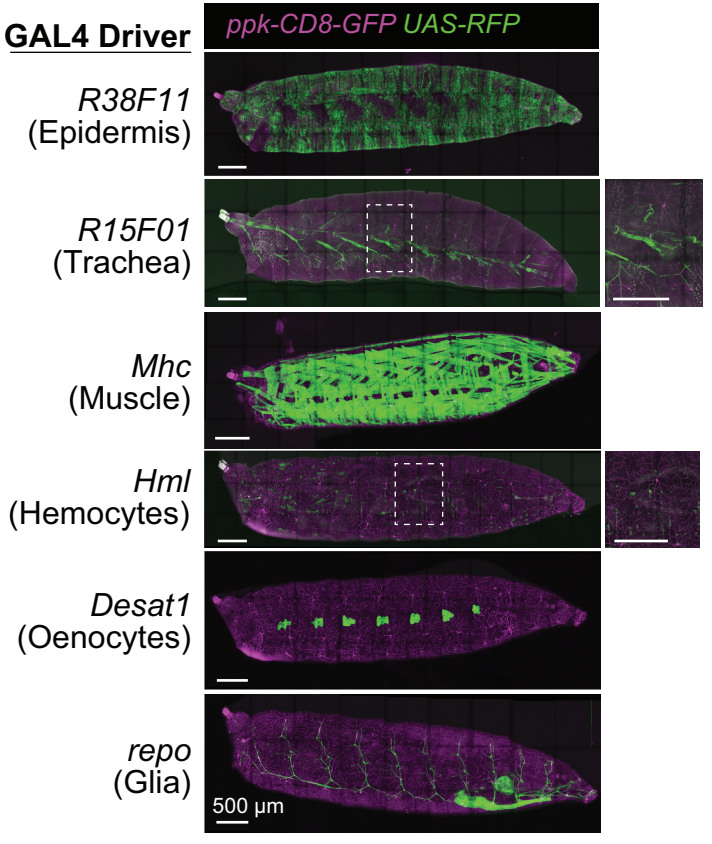

Figure 1 – figure supplement 2. Expression patterns of body wall GAL4 drivers. Related to Figure 1A. Maximum intensity projections of tiled confocal stacks show larval expression of membrane-targeted RFP (*UAS-mCD2-Cherry*) by the indicated drivers in larvae additionally expressing the C4da neuron-specific marker *ppk-CD8-GFP*. Scale bars, 500 µm. Genotypes: *ppk-mCD8-GFP/+; UAS-mCD2-Cherry/+; GAL4/+.*

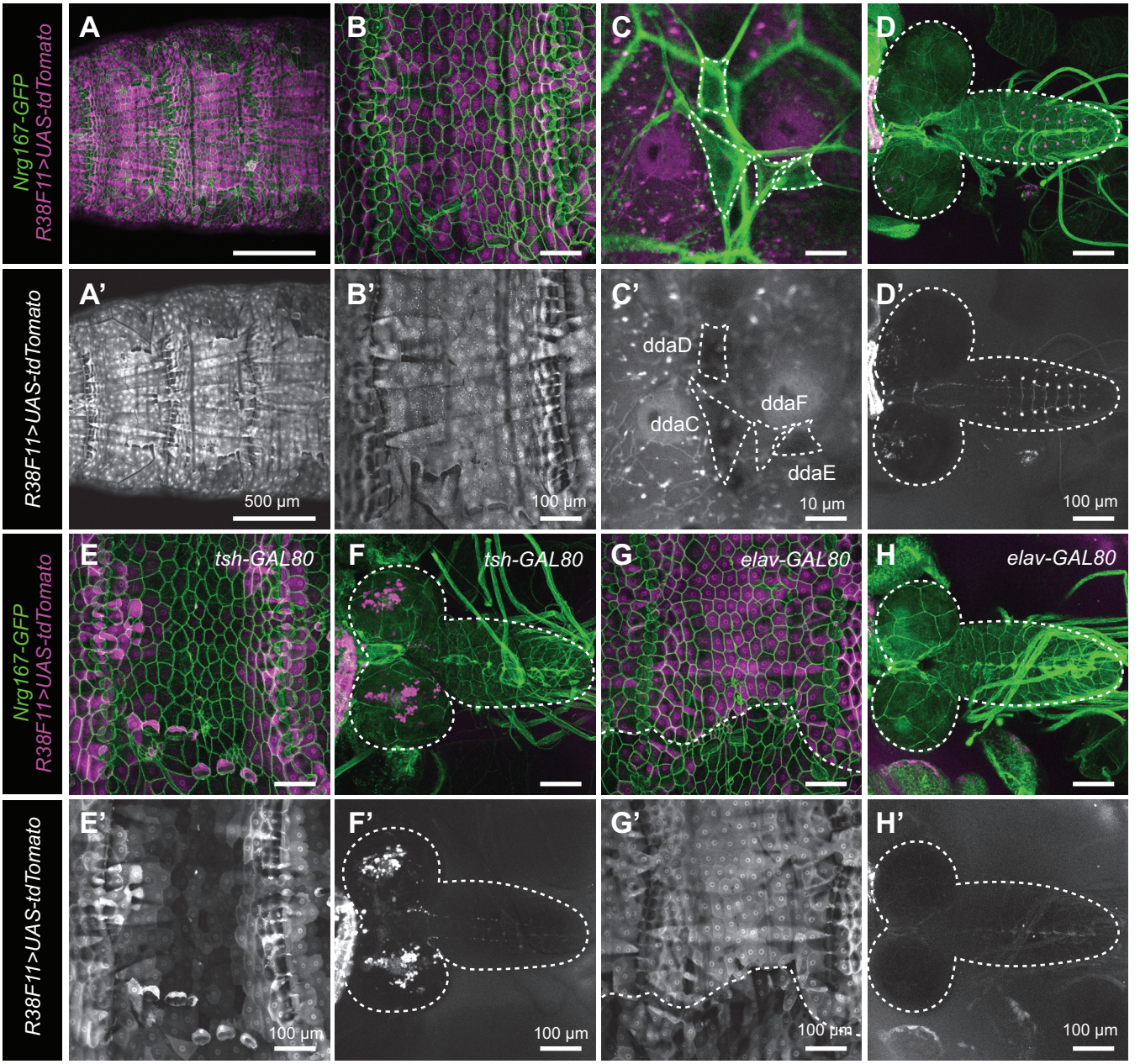

Figure 1 – figure supplement 3. Expression analysis of the pan-epidermal *R38F11-GAL4* driver. Related to Figures 1A and 1C. Maximum intensity projections of confocal stacks show larval expression of a red fluorescent protein (*UAS-td-Tomato*) under control of the indicated epidermal drivers in larvae expressing *Nrg^{167}-GFP*, an exon trap line that labels epidermal and glial membranes. (A-C) Peripheral expression patterns of *R38F11-GAL4*. Larvae are oriented dorsal-up. (A) Low-magnification view showing stereotyped expression in dorsal epidermis across multiple larval segments. *R38F11-GAL4* is likewise expressed throughout the ventral and lateral epidermis. Compared to other epidermal drivers (see Fig. 1S5), *R38F11-GAL4* exhibited more uniform expression. (B) *R38F11-GAL4* expression in dorsal epidermis of a single abdominal segment, A2. (C) High-resolution images of the larval skin territory containing dorsal cluster da neurons, which include the nociceptive neuron ddaC (outlined by dashed lines), mechanosensory neuron ddaF, and proprioceptive neurons ddaD/E. Note that although *R38F11-GAL4* is expressed in epidermal cells, expression is undetectable in da neurons. The *R38F11-GAL4* expression domain likewise excludes all other larval sensory neurons. (D) *R38F11-GAL4* expression in the larval CNS. *R38F11-GAL4* is expressed in a single motor neuron in each segment of the ventral ganglion, ~10 VNC interneurons, and ~50 additional neurons in each brain hemisphere. (E-H) GAL80-mediated refinement of *R38F11-GAL4* expression. (E) *Tsh-GAL80* induced variegation in epidermal *R38F11-GAL4* expression and (F) suppressed VNC expression while expanding brain expression domains of R38F11-GAL4. (G) Elav-GAL80 likewise induced epidermal variegation in *R38F11-GAL4* expression but (H) completely attenuated CNS expression. Dashed lines in (F, H) outline the larval brain and ventral ganglion. Genotypes: (A-D) *Nrg^{G00305}/+; UAS-tdTomato/+; R38F11-GAL4/+*, (E-F) *Nrg^{G00305}/+; UAS-tdTomato/tsh-GAL80; R38F11-GAL4/+*, (G-H) *Nrg^{G00305}/+; UAS-tdTomato/+; R38F11-GAL4/elav-GAL80.*

Yoshino et al, Fig. 1S4

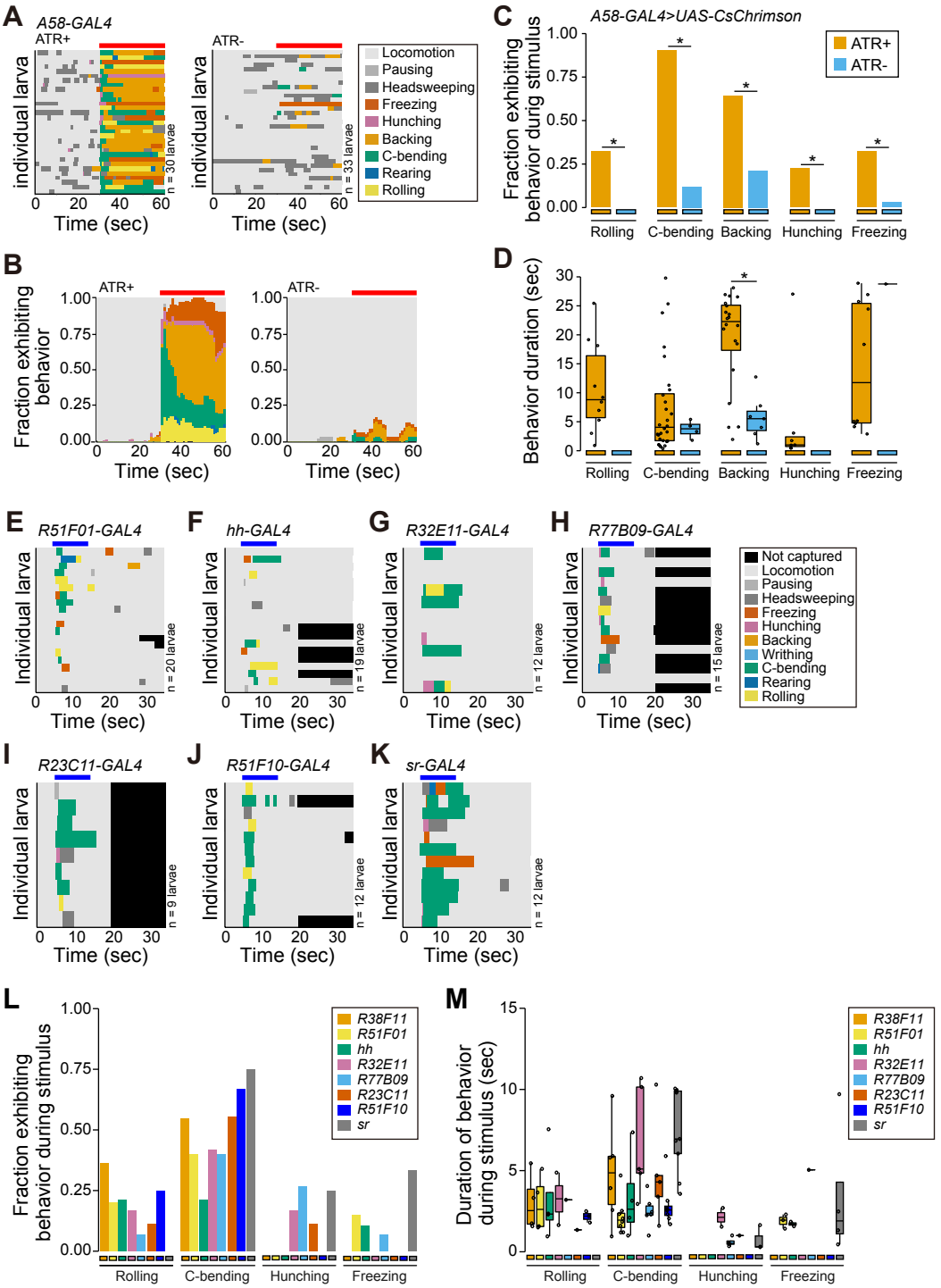

Figure 1 – figure supplement 4. Related to Figure 1B. (A-B) Behaivior ethograms of larvae following pan-epidermal stimulation (denoted with a red bar) mediated by *A58-GAL4*. (C) Fraction of larvae exhibiting indicated behaviors and (I) duration of indicated behaviors during optogenetic stimulation. (Genotype: *A58-GAL4, UAS-CsChrimson, tsh-GAL80, cha-GAL80/+*). (E-K) Behavior-al ethograms of larvae following optogenetic stimulation (denoted with a blue bar) with a panel of epidermal GAL4 drivers. (L) Fraction of larvae exhibiting indicated behaviors and (M) duration of indicated behaviors during light stimulus. Genotype: *GAL4, UAS-CsChrimson, elav-GAL80/+*.

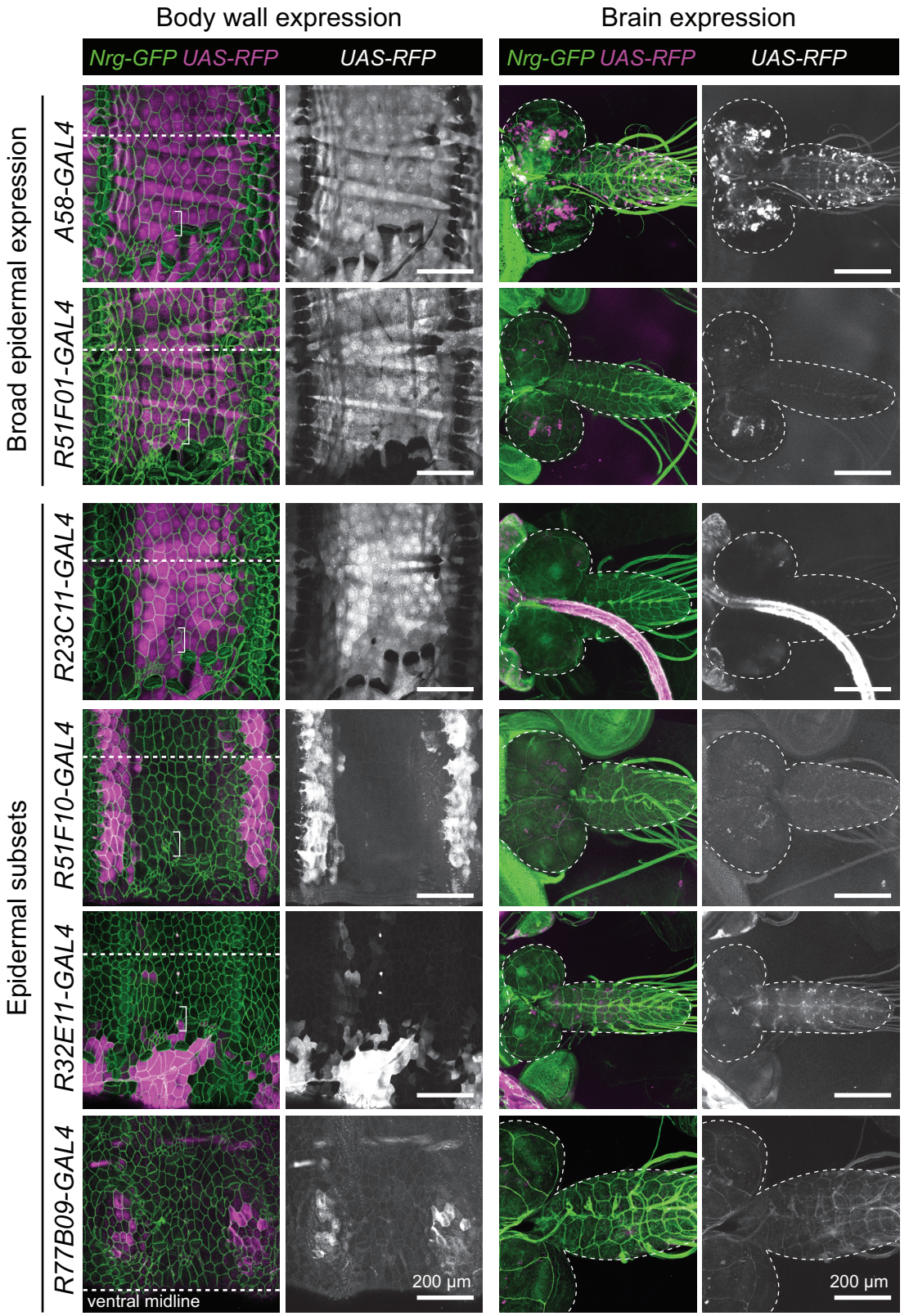

Figure 1 – figure supplement 5. Expression patterns of epidermal GAL4 drivers in the larval body wall and CNS. Related to Figure 1B. Maximum intensity projections of confocal stacks show larval expression of a red fluorescent protein (*UAS-tdTomato*) under control of the indicated epidermal drivers in larvae additionally expressing *Nrg*^{167}*-GFP*. White brackets mark the location of nociceptive C4da neuron cell bodies. Except for *A58-GAL4*, epidermal drivers used in this study exhibit sparse nervous system expression. Scale bars, 200 µm. Genotypes: *Nrg*^{G00305}*/+; UAS-tdTomato/+; GAL4/+.*

Yoshino et al, Fig. 2

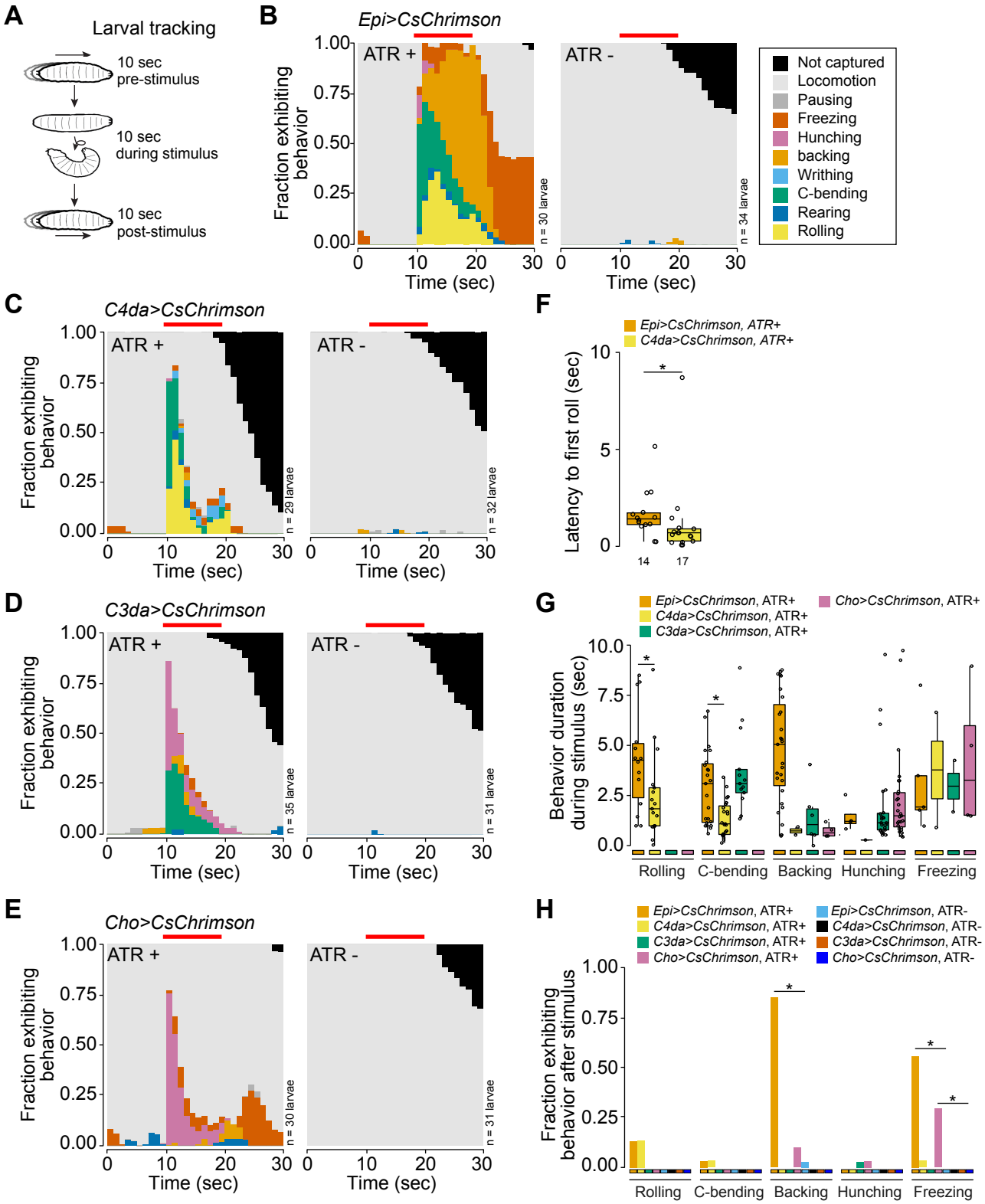

Figure 2. Stimulation of epidermal cells evokes multimodal behavioral responses. (A) Larval behaviors were scored for 10 sec before, during, and after optogenetic stimulation. (B-E) Fraction of larvae exhibiting indicated behaviors over time in one second bins expressing CsChrimson in (B) epidermal cells, (C) C4da, (D) C3da, and (E) Cho neurons in the presence and absence of all-trans retinal (ATR). Red line indicates the presence of light stimulation. (F) Latency to the first roll in responders from *Epi>Chrimson* ATR+ and *C4da>Chrimson* ATR+ treatment groups (n = 14, 17, respectively). (G) Duration of indicated behaviors in responders during optogenetic stimulation. (H) The fraction of larvae that exhibited indicated behaviors following removal of the light stimulus. Genotypes: *GAL4, UAS-CsChrimson/+*.

Yoshino et al, Fig. 2S1

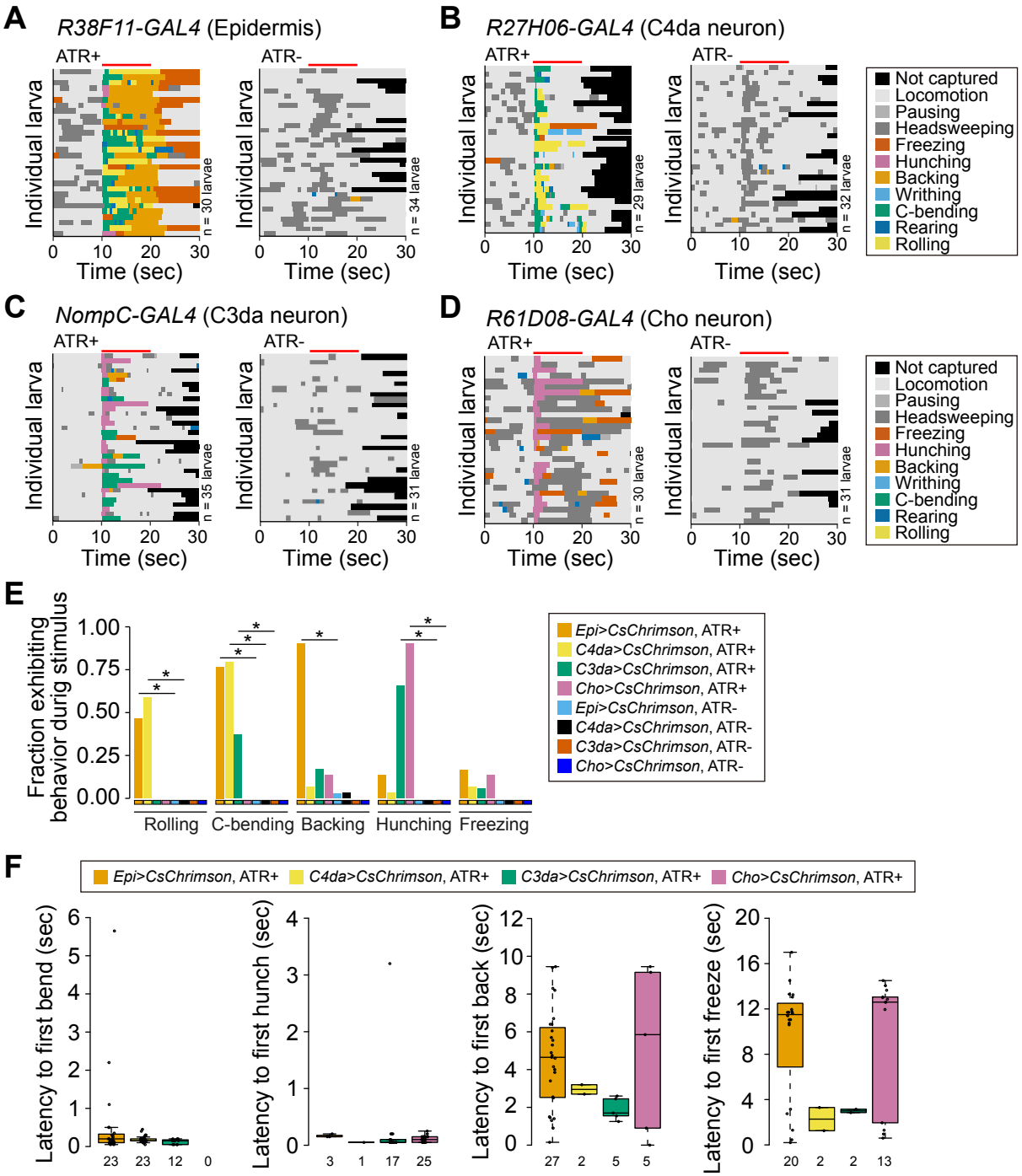

Figure 2 – figure supplement 1. (A-D) Behavior ethograms depict behaviors of individual larvae displayed in one second bins over the entire time course. (E) Fraction of larvae exhibiting indicated behaviors during light stimulus. (F) Latency to the first bend, hunch, back and freeze behaviors following optogenetic stimulation. Genotypes: *GAL4, UAS-CsChrimson/+*.

Yoshino et al, Fig. 3

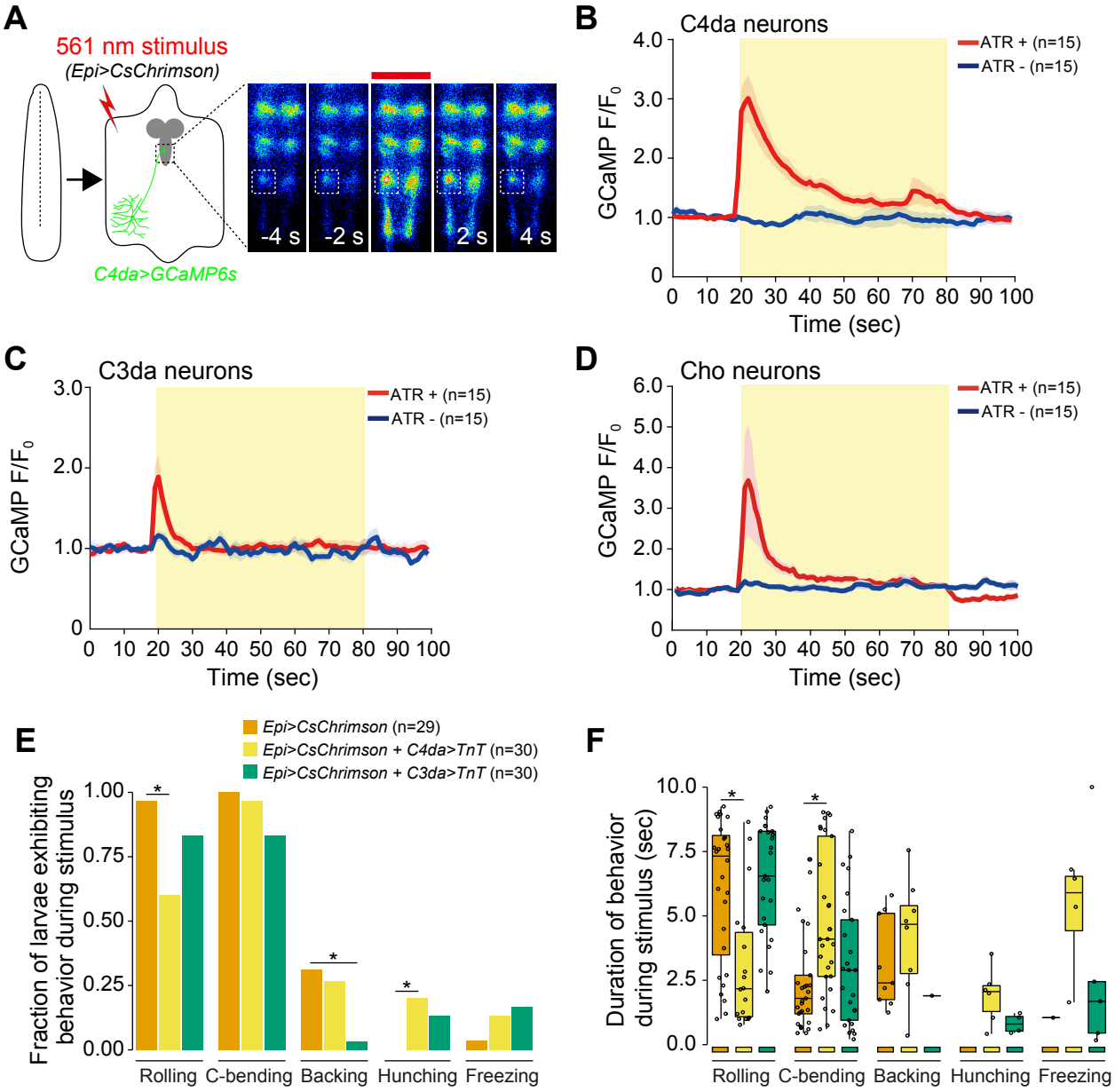

Figure 3. Epidermal stimulation drives SSN activation. (A) Optogentic activation of CsChrimson-expressing epidermal cells in the body wall triggers calcium transients in the axon terminal of GCaMP6s-expressing nociceptive SSNs. Images show responses from one representative animal. Plots depict mean GCaMP6s fluorescence intensity of the axon terminals of (B) C4da, (C) C3da, and (D) Cho neurons following optogenetic activation (light stimulus, yellow box) of epidermal cells over time. Solid lines depict mean GCaMP6s fluorescence across replicates (n=15 larval fillet preparations), shading indicates SEM, red traces are ATR+ and blue, ATR-. (E) The fraction of larvae exhibiting indicated behaviors during optogenetic epidermal stimulation in combination with SSN silencing via Tetanus Toxin (TnT) expression. (F) The duration of the behavioral responses during optogenetic epidermal stimulation with neuronal TnT expression. Genotypes: (A-C) *AOP-GCaMP6s, UAS-CsChrimson; R38F11-GAL4/+* together with the following LexA drivers: *R27H06-LexA* (C4da neurons), *NompC-LexA* (C3da neurons); (D) *UAS-GCaMP6s, AOP-CsChrimson, R61D08-GAL4/R38F11-LexA*; (E-F) *R38F11-GAL4, UAS-CsChrimson, AOP-LexA-TnT/+* (*Epi>CsChrimson*); *R38F11-GAL4, UAS-CsChrimson, AOP-LexA-TnT/ppk-LexA* (*Epi>CsChrimson + C4da>TnT*); *R38F11-GAL4, UAS-CsChrimson, AOP-LexA-TnT/NompC-LexA* (*Epi>CsChrimson + C3da>TnT*).

Yoshino et al, Fig. 3S1

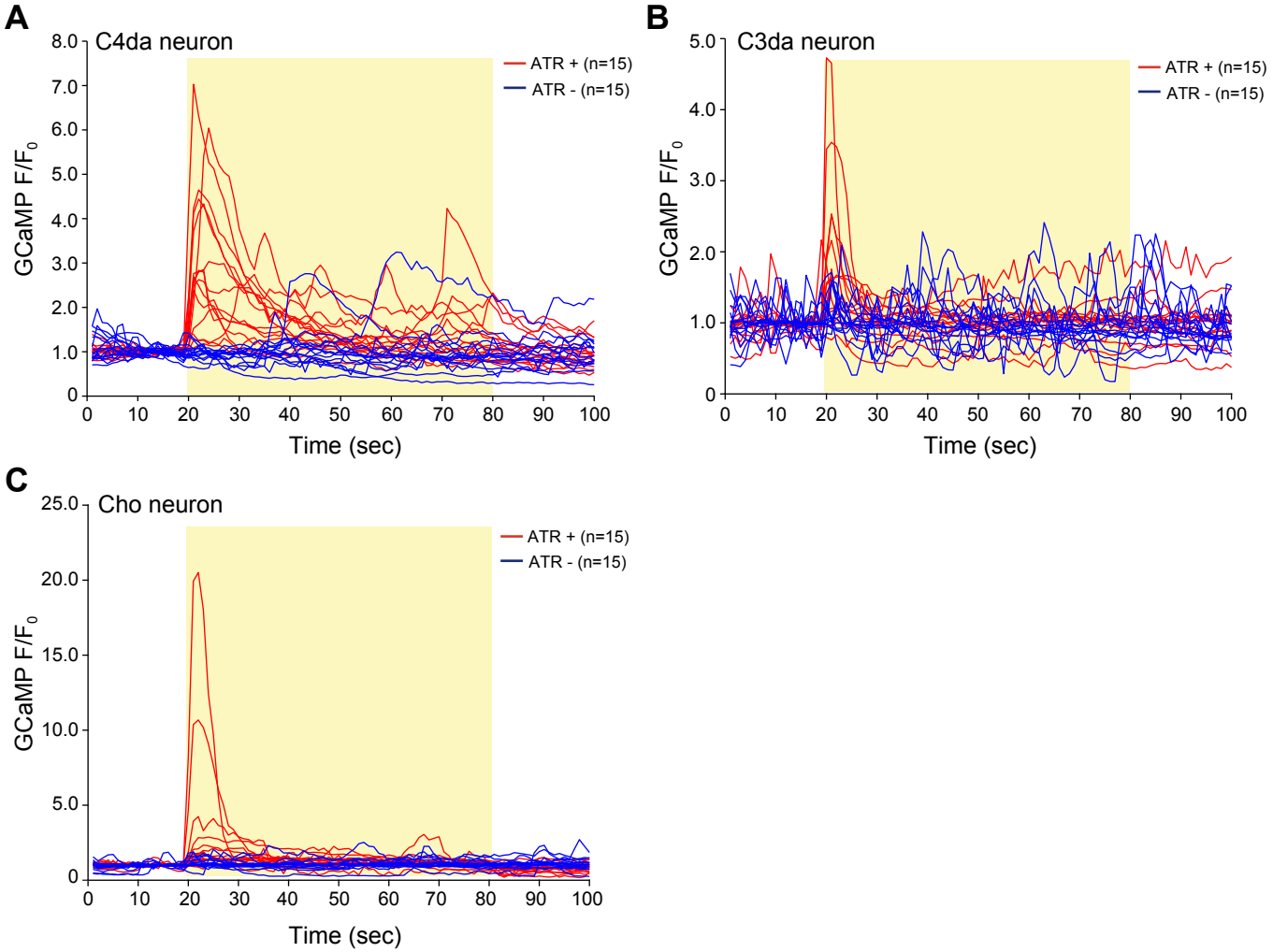

Figure 3 – figure supplement 1. Related to Figure 3A-3D. GCaMP6s responses in axon terminals of (B) C4da, (C) C3da, and (D) Cho neurons following optogenetic activation (light stimulus, yellow box) of epidermal cells over time. Each trace represents the GCaMP6s fluorescence of an individual larval fillets. Red traces are ATR+ and blue, ATR-.

Yoshino et al, Fig. 3S2

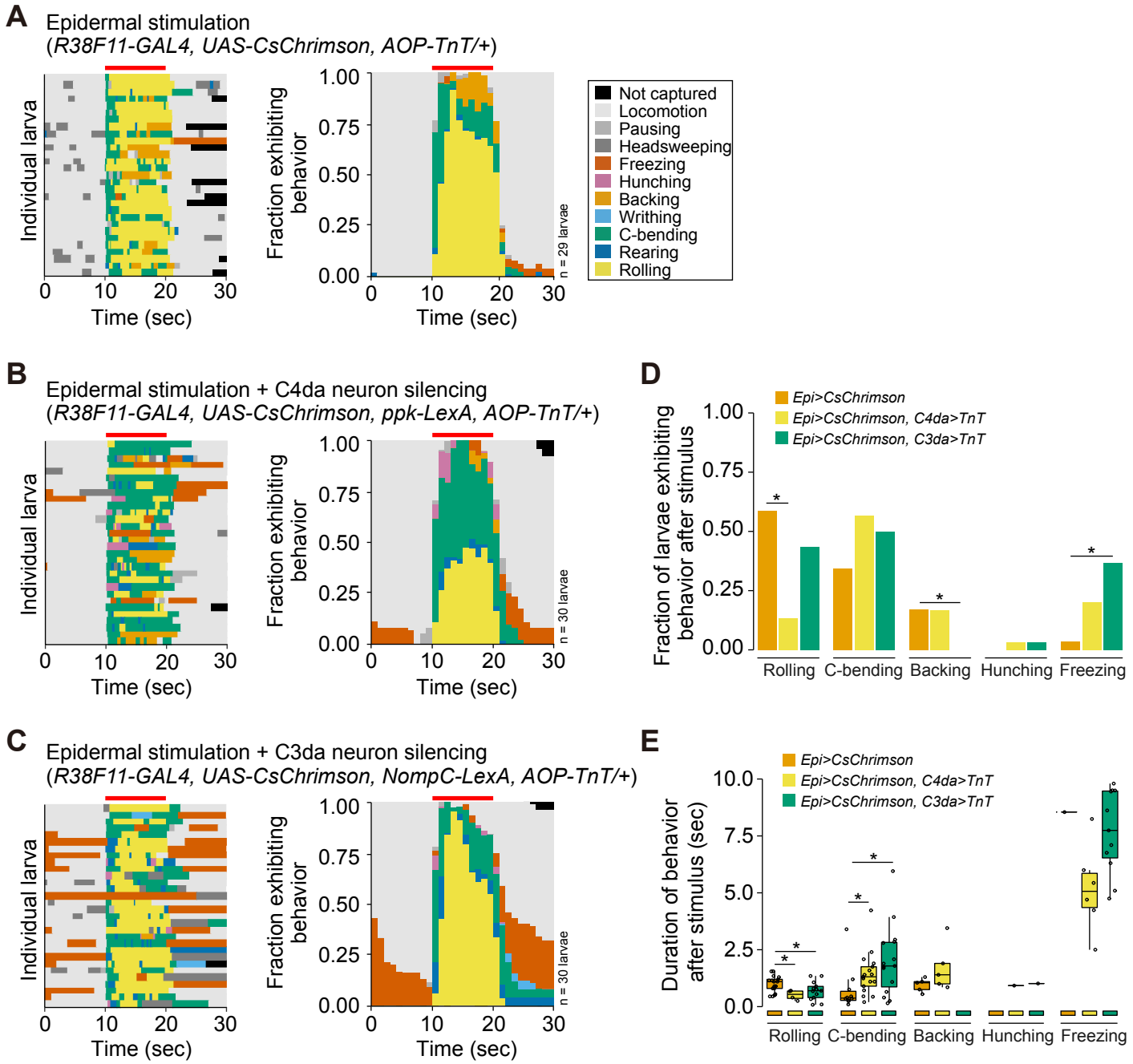

Figure 3 – figure supplement 2. Related to Figure 3E-3F. (A-C) Behavior ethograms (left) and fraction of larvae (right) exhibiting indicated behaviors to optogenetic epidermal stimulation in combination with (A) an *AOP-TNT* transgene (control lacking LexA driver), (B) C4da neuron silencing via Tetanus Toxin (TnT), and (C) C3da neuron silencing via TnT. (D) Fraction of larvae exhibiting each behavior and (E) the duration of behavior responses after removal of the light stimulus. Genotypes are indicated in (A-C).

Yoshino et al, Fig. 4

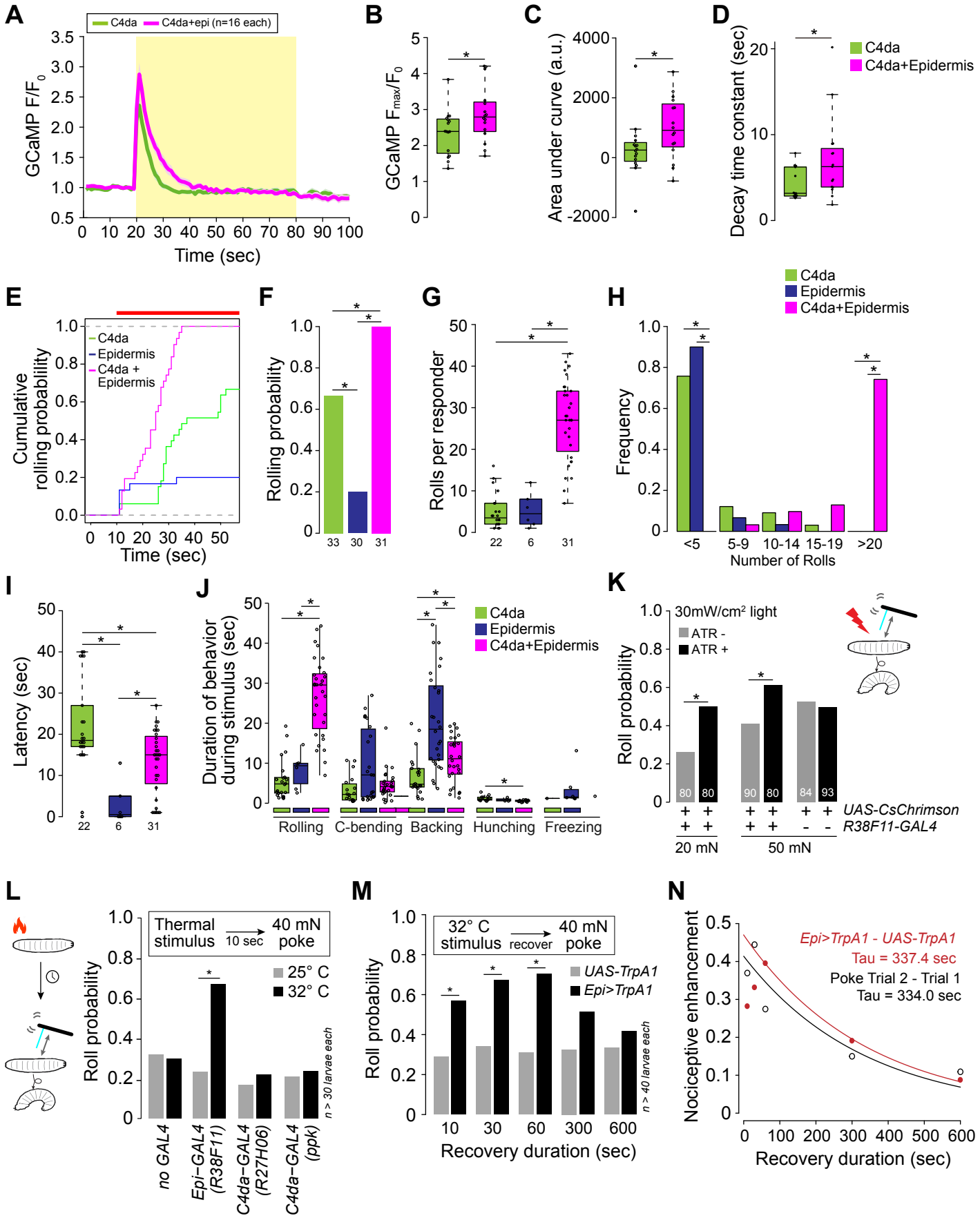

Yoshino et al, Fig. 4

Figure 4. Epidermal stimulation augments nociceptive responses. (A) Mean GCaMP6s responses (F/F0) in C4da axons during optogenetic stimulation (yellow box) of C4da neurons alone (green) or of C4da neurons and epidermal cells (magenta), shading indicates SEM. (B) Simultaneous epidermal stimulation increased the peak calcium response (Fmax/F0), (C) total calcium influx (area under the curve), and (D) duration of C4da neuron calcium responses compared to stimulation of C4da neurons alone. Genotypes: *ppk-LexA, AOP-GCAMP6s/+; R27H06-GAL4/UAS-CsChrimson* (C4da) and *ppk-LexA, AOP-GCAMP6s/+; R27H06-GAL4/R38F11-GAL4, UAS-CsChrimson* (C4da+epi). (E-J) Characterization of the behavioral responses to low-intensity optogenetic stimulation of C4da neurons, epidermal cells, or simulteanous C4da neurons and epidermal cells. (E) Cumulative and (F) total roll probability during optogenetic stimulation (indicated by the red bar). n = 33 (*C4da>CsChrimson*), 30 (*Epi>CsChrimson*), and 31 (*C4da + Epi>CsChrimson*) larvae. (G, H) Number and frequency distribution of rolls, (I) latency to the first roll observed for larvae of the indicated genotypes, and (J) the duration of the indicated behaviors during light stimulus. Genotypes: *UAS-CsChrimson/+; R27H06-GAL4/+* (C4da), *UAS-CsChrimson/+; R38F11-GAL4/+* (Epidermis), *UAS-CsChrimson/+; R27H06-GAL4/R38F11-GAL4* (C4da+Epidermis). (K) Roll probability of larvae to a 20 mN or 50 mN von Frey mechanical stimulus and epidermal optogenetic activation (a light stimulus, 30mW/cm2 that was insufficient on its own to induce nocifensive rolling). Larvae were reared in the presence or absence of ATR, as indicated. Genotypes: *UAS-CsChrimson/+; R38F11-GAL4/+*. (L-N) Prior epidermal but not nociceptor stimulus potentiates mechanical nociceptive responses. (L) Roll probability of control larvae (*UAS-TrpA1/+*) or larvae expressing TrpA1 in the epidermis (*Epi-GAL4: R38F11-GAL4*) or C4da neurons (*UAS-TrpA1/+; C4da-GAL4 #1: R27H06-GAL4, UAS-TrpA1/+; C4da-GAL4 #2: ppk-GAL4, UAS-TrpA1/+*), or control larvae (no GAL4: *UAS-TrpA1/+;*) in response to 40 mN mechanical stimulus 10 sec following 10 sec of a thermal stimulus (25º or 32º C). To control for effects of genetic background, we confirmed that each of the experimental genotypes exhibited mechanically induced nociceptive sensitization (Fig. 4S1C). (M) Roll probability of control larvae (*UAS-TrpA1/+*) or larvae expressing TrpA1 in the epidermis (*Epi>TrpA1: R38F11-GAL4, UAS-TrpA1/+*) in response to a 40 mN mechanical stimulus delivered at the indicated time interval following a 32º C thermal stimulus. (N) Nociceptive enhancement (difference in the roll probablity to the first and second stimulus) is plotted against the recovery duration and results were fit to an exponential curve to derive the decay time constant. The red line indicates nociceptive enhancement of a mechanical stimulus by a prior epidermal thermogenetic stimulus; the black line indicates nociceptive enhancement by a prior mechanical stimulus.

Yoshino et al, Fig. 4S1

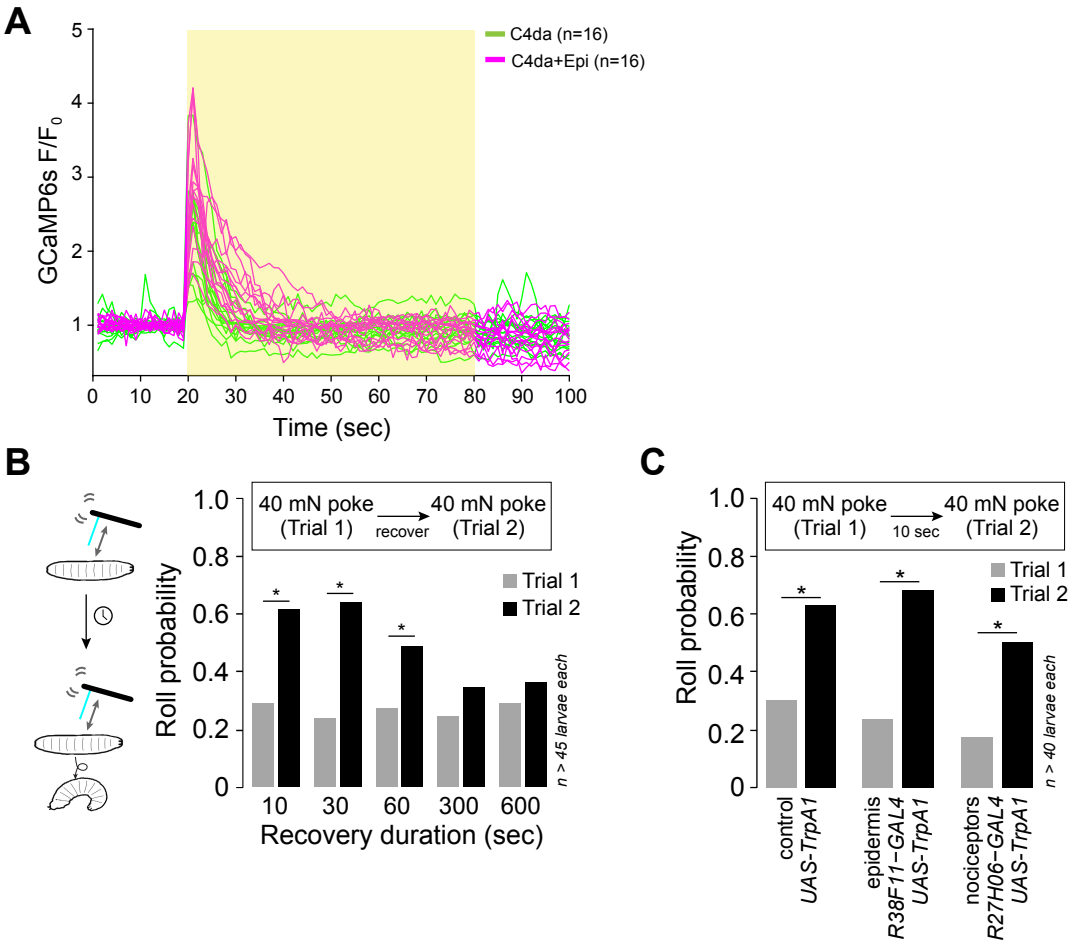

Figure 4 – figure supplement 1. (A) GCaMP6s responses (F/F0) of individual replicates during optogenetic stimulation (yellow box) of C4da neurons alone (green) or C4da neurons and epidermal cells (magenta), yellow box indicates presence of light stimulus. Genotypes: *ppk-LexA, AOP-GCAMP6s/+; R27H06-GAL4/UAS-CsChrimson* (C4da) and *ppk-LexA, AOP-GCAMP6s/+; R27H06-GAL4/ R38F11-GAL4, UAS-CsChrimson* (C4da+epi). (B) Roll probability of larvae in response to two successive 40 mN mechanical stimuli spaced by the indicated amount of time (recovery duration). Genotype: *R38F11-GAL4/+*. (C) Roll probability of larvae expressing *UAS-TrpA1* in nociceptors exhibited levels of mechanically induced nociceptive potentiation comparable to other experimental genotypes used in the study (control: *UAS-TrpA1/+*; epidermis: *R38F11-GAL4, UAS-TrpA1/+*; nociceptors: *R27H06-GAL4, UAS-TrpA1/+*).

Yoshino et al, Fig. 5

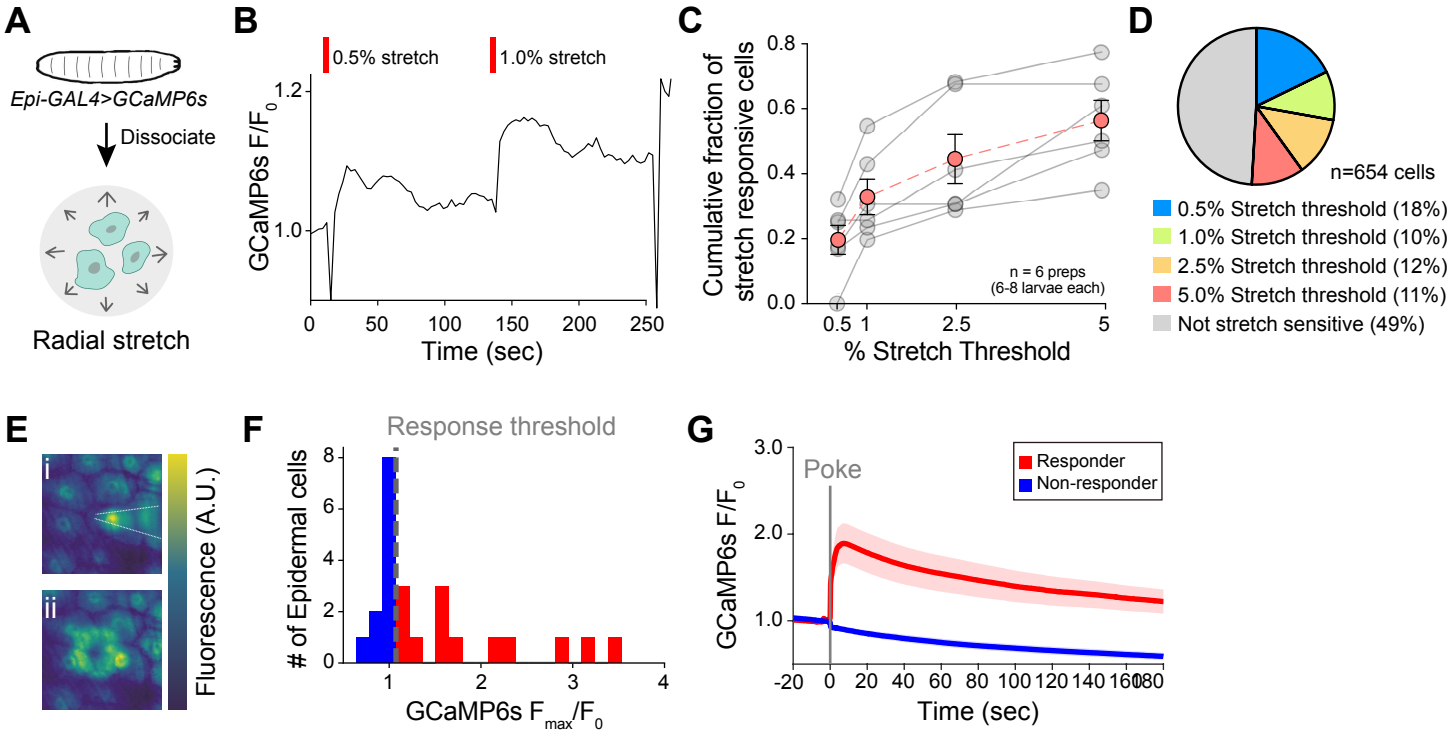

Figure 5. Epidermal cells are intrinsically mechanosensitive. (A) Schematic of preparation to measure radial stretch evoked calcium responses of dissociated epidermal cells. (B) Representative calcium responses of a dissociated epidermal cell to 0.5 and 1% radial stretch. (C) Dose response curve displaying the fraction of epidermal cells activated by increasing magnitudes of stretch. Red trace displays the mean ± SEM across six independent dissociated cell preparations, obtained from a minimum of 6 larvae. Gray traces display fraction responding in each dissociated cell preparation replicate. (D) Subsets of epidermal cells display varying stretch thresholds, n = 6 dissociated cell preparations, for a total of 654 epidermal cells. (E) Representative mechanically induced epidermal calcium responses in the larval body wall. Images show GCaMP6s fluorescence intensity 100 msec prior to (i) and 20 sec following (ii) a 25 µm membrane displacement (poke). (F) Distribution of the peak calcium response (Fmax/F0) to a 25 µm membrane displacement (poke) of 24 cells from 24 independent larval fillets. Cells were classified as responders (>10% increase in normalized GCaMP6s fluorescence). (G) Mean calcium responses (F/F0) of poke responders and non-responders (n = 12 cells each). Solid lines depict mean normalized GCaMP6s fluorescence and shading indicates SEM. Genotype: *R38F11-GAL4, UAS-GCaMP6s*.

Yoshino et al, Fig. 5S1

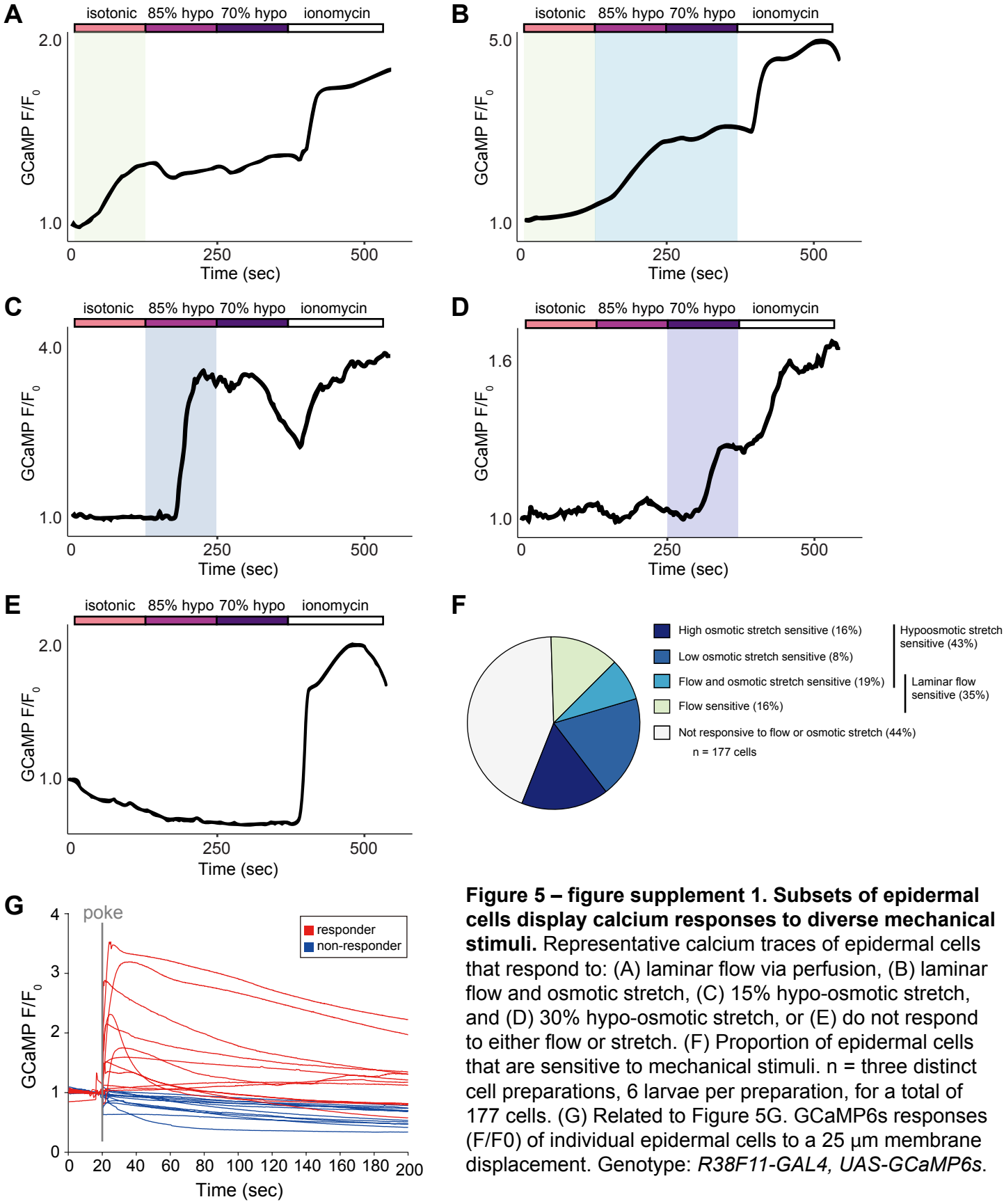

Figure 5 – figure supplement 1. Subsets of epidermal cells display calcium responses to diverse mechanical stimuli. Representative calcium traces of epidermal cells that respond to: (A) laminar flow via perfusion, (B) laminar flow and osmotic stretch, (C) 15% hypo-osmotic stretch, and (D) 30% hypo-osmotic stretch, or (E) do not respond to either flow or stretch. (F) Proportion of epidermal cells that are sensitive to mechanical stimuli. n = three distinct cell preparations, 6 larvae per preparation, for a total of 177 cells. (G) Related to Figure 5G. GCaMP6s responses (F/F0) of individual epidermal cells to a 25 µm membrane displacement. Genotype: *R38F11-GAL4, UAS-GCaMP6s*.

Yoshino et al, Fig. 6

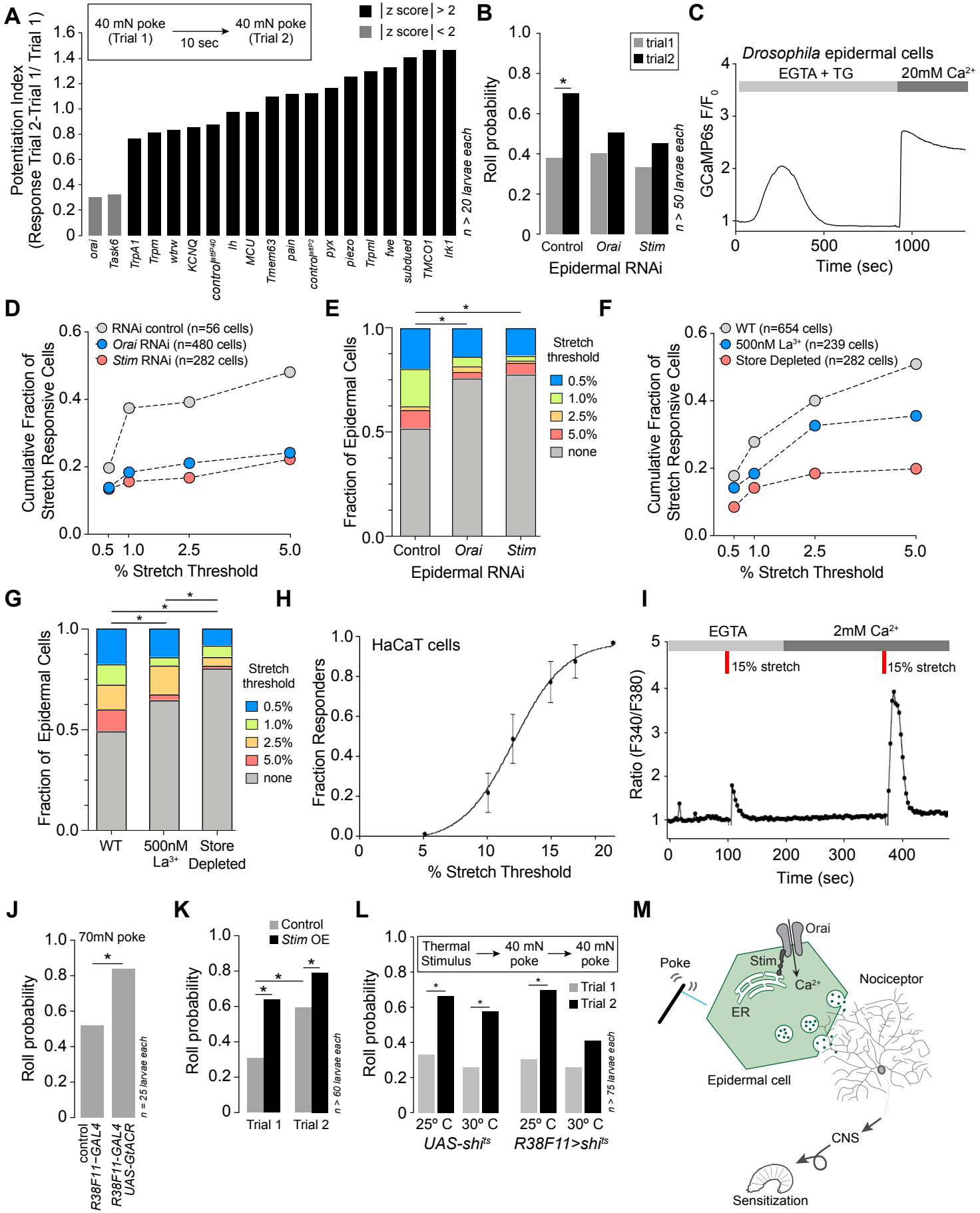

Yoshino et al, Fig. 6

Figure 6. CRAC channels are required for epidermal mechanosensory responses and epidermal nociceptive potentiation. (A) RNAi screen for epidermal ion channels required for mechanically induced nociceptive potentiation. Bars depict nociceptive potentiation index (difference in the larval roll probability to the first and second mechanical stimuli divided by roll probability to the first mechanical stimulus). Candidate channels were chosen for further analysis if they had a a z-score greater than 2 (absolute value). (B) The CRAC channels Orai and Stim are required in epidermal cells for mechanically evoked nociceptive potentiation. Roll probability of larvae of the indicated genotypes (Control RNAi, *R38F11-GAL4, UAS-RFP-RNAi/+*; *Stim* RNAi, *R38F11-GAL4, UAS-Stim-RNAi/+*; *Orai* RNAi, *R38F11-GAL4, UAS-Orai-RNAi/+*) to a 40 mN mechanical stimulus followed by a second 40mN mechanical stimulus 10 sec later. (C) *Drosophila* epidermal cells display classical store-operated calcium entry (SOCE). Treatment with the drug thapsigargin (TG) in the absence of extracellular calcium promoted depletion of intracellular calcium stores and calcium influx, following extracellular calcium re-addition. (D-E) The fraction of stretch-sensitive epidermal cells is significantly decreased in cells isolated from larvae expressing *Stim* RNAi, or *Orai* RNAi, as compared to control RNAi. (F-G) The Orai blocker, lanthanum chloride (500 nM) or the depletion of intracellular stores by thapsigargin (1 μM) reduces the fraction of stretch-sensitive epidermal cells. (H) Stretch stimuli evoke dose-dependent calcium signals in the human keratinocyte HaCaT cell line. (I) Representative stretch-evoked SOCE calcium response in HaCaT cells. Stretch induces calcium release from stores in the absence of extracellular calcium and a greater calcium influx in the presence of extracellular calcium. (J) Epidermal hyperpolarization enhances mechanical nocifensive responses. Roll probability of larvae expressing GtACR in epidermal cells (*R38F11-GAL4, UAS-GtACR/+*) or control larvae (*R38F11-GAL4/+*) to a single 70 mN mechanical stimulus. (K) Epidermal Stim overexpression enhances mechanical nocifensive responses. Roll probability of Stim-overexpressing larvae (*R38F11-GAL4, UAS-Stim/+*) and control larvae (*R38F11-GAL4/+*) to two successive 40 mN mechanical stimuli delivered 10 sec apart. (L) Epidermal potentiation of mechanical nociceptive responses requires exocytosis. Roll probability of control larvae (*UAS-shi^{ts}/+*) or larvae expressing temperature-sensitive dominant-negative shibire in epidermal cells (*R38F11-GAL4, UAS-shi^{ts}/+*) in response to two successive mechanical stimuli that followed conditioning at the permissive (25º C) or non-permissive (30º C) temperature. (M) Model of epidermal-neuronal signaling. Mechanically evoked Stim/Orai calcium signaling in epidermal cells drives calcium influx and vesicle release that drives nociceptor activation and mechanical sensitization via activation of C4da nociceptors.

Yoshino et al, Fig. 6S1

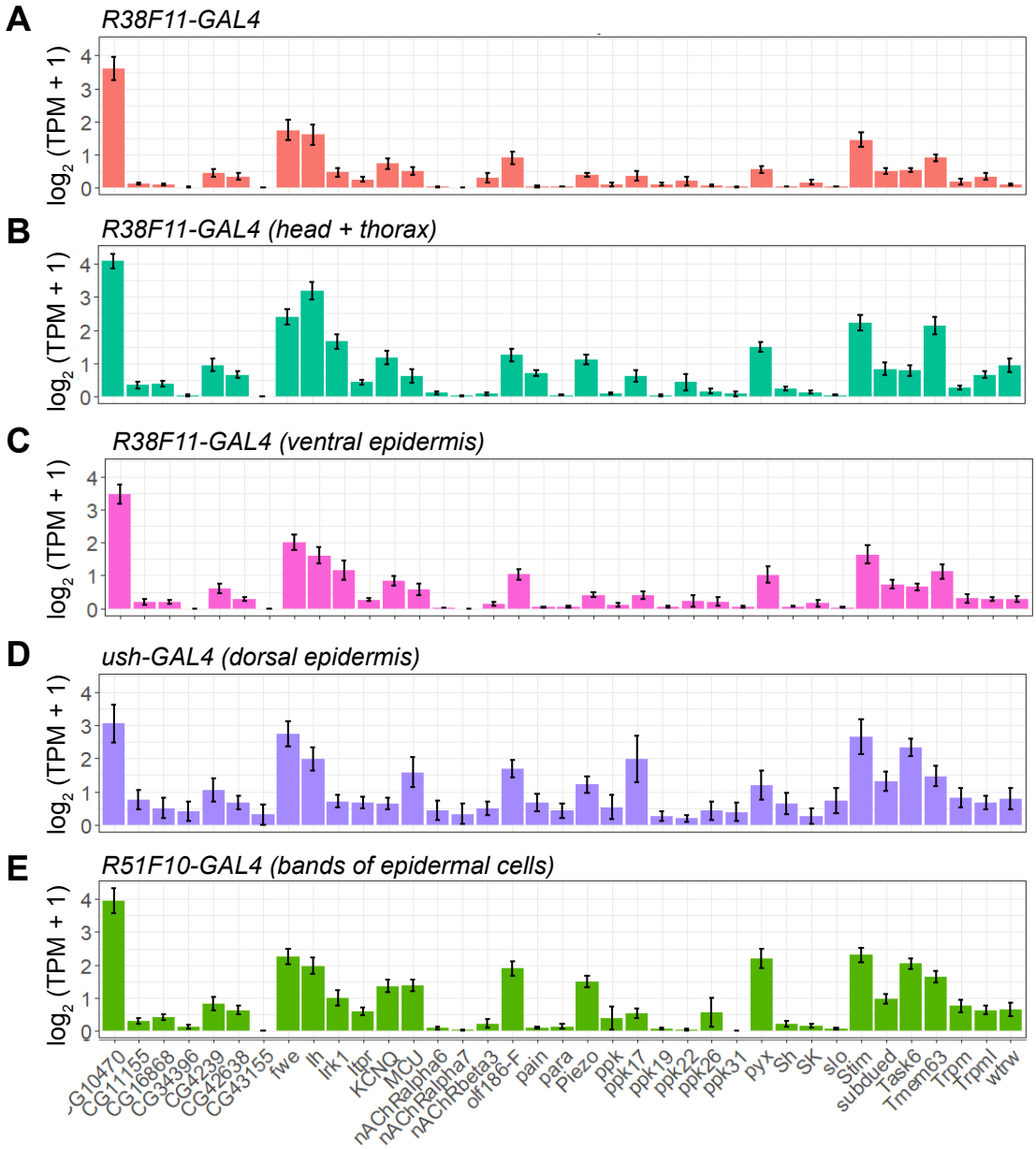

Figure 6 – figure supplement 1. Ion channel expression in epidermal cells. Related to Figure 6A. Five populations of UAS-GFP-expressing epidermal cells were selected for RNA-seq analysis. GFP-positive epidermal cells were dissociated into single cell suspensions, manually picked, and subjected to RNA-Seq analysis. Plots depict expression levels (mean +/- standard deviation) of the indicated ion channels (log2(TPM+1)) from n > 6 independent libraries for each sample type.
(A) Expression in epidermal cells collected from *R38F11-GAL4* which labels all epidermal cells. (B) Anatomically defined subsets of epidermal cells were profiled by removing posterior segments from *R38F11-GAL4, UAS-GFP* larvae (*R38F11-GAL4* head and thorax) or (C) dissecting the ventral epidermis (*R38F11-GAL4* ventral epidermis). (D) Expression in the dorsal epidermis (*ush-GAL4*) and or (E) bands of epidermal cells (*R51F10-GAL4*).

Yoshino et al, Fig. 6S2

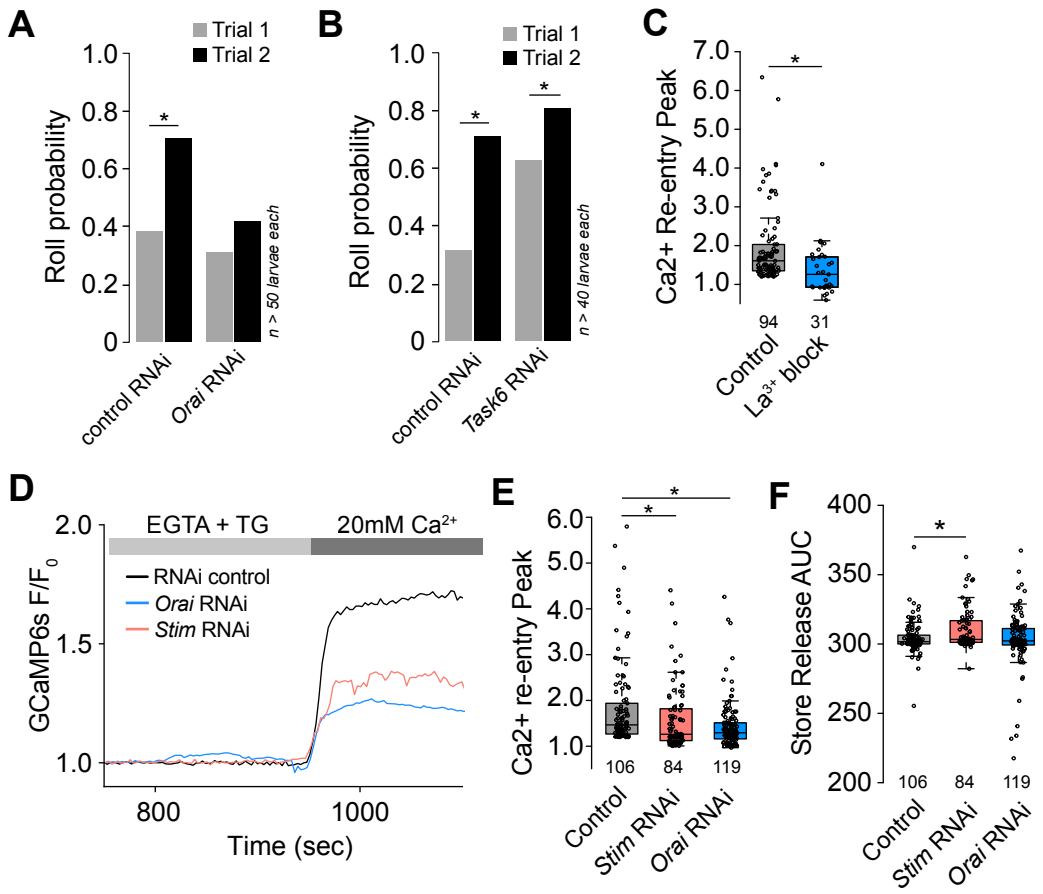

Figure 6 – figure supplement 2. (A-B) Epidermal knockdown of ion channels affects larval mechanical nociceptive responses. Roll probability in response to the first and second mechanical stimulus for larvae expressing RNAi transgenes to (A) *Orai* or *attP40* RNAi control transgene and (B) *Task6* or *attP2* RNAi control transgene. (C) Epidermal cell SOCE is attenuated by pre-treatment with the Orai blocker, lanthanum chloride (100 nM). (D) Representative SOCE after treatment with TG (1 μM) in epidermal cells isolated from larvae treated with control RNAi, *Stim* RNAi (red), or *Orai* RNAi, (blue). (E) Peak calcium response following SOCE in epidermal cells isolated from larvae treated with control RNAi, *Stim* RNAi (red), or *Orai* RNAi, (blue). (F) *Stim* RNAi decreases calcium store content of epidermal cells. Calcium store content was measured as the area under the curve of the cytosolic calcium response to TG (1 μM) in the absence of extracellular calcium.

Table S1. Alleles used in this study

Transgene / Allele	Uses / Features	Identifier (RRID)
A58-GAL4	GAL4 driver (epidermis)	Flybase_FBal0181674
Desat1-GAL4	GAL4 driver (oenocytes)	BDSC_65405
GMR15F01-GAL4	GAL4 driver (trachea)	BDSC_45071
GMR23C11-GAL4	GAL4 driver (epidermis)	BDSC_45123
GMR27H06-GAL4	GAL4 driver (C4da neurons)	BDSC_49440
GMR32E11-GAL4	GAL4 driver (epidermis)	BDSC_48109
GMR38F11-GAL4	GAL4 driver (epidermis)	BDSC_50014
GMR51F01-GAL4	GAL4 driver (epidermis)	BDSC_38787
GMR51F10-GAL4	GAL4 driver (epidermis)	BDSC_38793
GMR61D08-GAL4	GAL4 driver (Cho neurons)	BDSC_39272
GMR77B09-GAL4	GAL4 driver (epidermis)	Flybase_FBti0138381
hh-GAL4	GAL4 driver (epidermis)	DGGR_118117
Hml-GAL4	GAL4 driver (hemocytes)	BDSC_6395
MHC-GAL4	GAL4 driver (muscle)	BDSC_55132
NompC-GAL4	GAL4 driver (C3da neurons)	BDSC_36361
Piezo-GAL4	GAL4 driver (Piezo-expressing cells)	BDSC_78335
ppk-GAL4	GAL4 driver (C4da neurons)	BDSC_32079
repo-GAL4	GAL4 driver (glia)	BDSC_7415
sr-GAL4	GAL4 driver (apodemes)	BDSC_26663
ppk-LexA	LEXA driver (C4da neurons)	Flybase_FBtp0125814
NompC-LexA	LEXA driver (C3da neurons)	BDSC_52241
elav-GAL80	GAL80 (pan-neuronal)	Flybase_FBtp0079702
tsh-GAL80	GAL80 (VNC)	Flybase_FBti0114123
ush-GAL4	GAL4 driver (epidermis)	BDSC_36524
Nrg167GFP	Reporter (epidermal cell junctions)	BDSC_6844
UAS-tdTomato	Reporter (RFP)	BDSC_36328
UAS0GCaMP6s	Reporter (Calcium indicator)	BDSC_42749
UAS-GCaMP6s	Reporter (Calcium indicator)	BDSC_42746
AOP-GCaMP6s	Reporter (Calcium indicator)	BDSC_44273
AOP-TNT	Neuronal silencing (Tetanus Toxin)	Flybase_FBtp0144631
UAS-shi-ts	Temperature-sensitive Dynamin	BDSC_44222
UAS-CsChrimson	Inducible Cation Channel	BDSC_55135
UAS-CsChrimson	Inducible Cation Channel	BDSC_55136
UAS-TRPA1	Inducible Cation Channel	BDSC_26263
UAS-GtACR	Inducible Anion Channel	BDSC_92983
UAS-luciferase RNAi	RNAi transgene	BDSC_31603
UAS-RFP-RNAi	RNAi transgene	BDSC_67852
UAS-fwe-RNAi	RNAi transgene	BDSC_27323
UAS-Ih-RNAi	RNAi transgene	BDSC_29574
UAS-Ih-RNAi	RNAi transgene	BDSC_58089
UAS-Irk1-RNAi	RNAi transgene	BDSC_42644
UAS-KCNQ-RNAi	RNAi transgene	BDSC_80446
UAS-MCU-RNAi	RNAi transgene	BDSC_67897

UAS-orai-RNAi	RNAi transgene	BDSC_53333
UAS-orai-RNAi	RNAi transgene	VDRC_12221
UAS-pain-RNAi	RNAi transgene	BDSC_51835
UAS-piezo-RNAi	RNAi transgene	FlyBase_FBst0457216
UAS-piezo-RNAi	RNAi transgene	Flybase_FBtp0071516
UAS-pyx-RNAi	RNAi transgene	BDSC_31297
UAS-stim-RNAi	RNAi transgene	BDSC_41759
UAS-stim-RNAi	RNAi transgene	FlyBase_FBst0478081
UAS-subdued-RNAi	RNAi transgene	FlyBase_FBst0480747
UAS-Task6-RNAi	RNAi transgene	BDSC_28016
UAS-Task6-RNAi	RNAi transgene	FlyBase_FBst0471360
UAS-Tmem63-RNAi	RNAi transgene	FlyBase_FBst0470667
UAS-TMCO1-RNAi	RNAi transgene	BDSC_42896
UAS-TMCO1-RNAi	RNAi transgene	BDSC_55909
UAS-TrpA1-RNAi	RNAi transgene	BDSC_66905
UAS-Trpm-RNAi	RNAi transgene	BDSC_31291
UAS-Trpml-RNAi	RNAi transgene	BDSC_31294
UAS-wtrw-RNAi	RNAi transgene	BDSC_51563

Table S2. Larval behaviors scored in this study

Behavior	Description / Criteria
Locomotion	Continuous forward movement with smooth, regular peristalsis
Pausing	Break in locomotion, lasting less than 1 second
Freezing	Break in locomotion that persists for longer than 1 second
Hunching	Contraction along the anterior-posterior axis; no forward / backward motion or curling
Backward locomotion	Anterior-to-posterior peristalsis accompanied by movement in reverse
Writhing crawl	Forward movement with anterior and posterior sweeping of the body, tilting onto the side axis
C-bending	Bending into a c-shape, with both head and tail bending in the same direction; includes incomplete rolls
Rearing	Upwards bending or arching of anterior part of the body, with posterior part largely stationary
Rolling	Larva completes a full 360-degree rotation of its body

Table S3. Solutions used in Calcium imaging studies.

***Drosophila* saline** (adapted from Niemeyer et al 1996)			
Compound	**M.W. (g/mol)**	**1X Concentration (mM)**	**For 1L (1X)**
NaCl	58.44	120	7.013 g
KCl	74.55	5	0.373 g
Proline	115.13	5	0.576 g
HEPES	238.30	10	2.383 g
Trehalose	378.33	5	3.78 g
Sucrose	342.30	32.5	11.125 g
CaCl2	1M stock	1.5	1.5 ml from 1M stock
MgCl2	1M stock	1	1 ml from 1M tock
		pH (with NaOH)	7.15
		Osmolarity (mOsm/L)	310

EGTA / "Zero Ca2+"			
Compound	**M.W. (g/mol)**	**1X Concentration (mM)**	**For 1L (1X)**
NaCl	58.44	120	7.013 g
KCl	74.55	5	0.373 g
Proline	115.13	5	0.576 g
HEPES	238.30	10	2.383 g
Trehalose	378.33	5	3.78 g
Sucrose	342.30	32.5	11.125 g
EGTA	380.35	1.5	0.571 g
MgCl2	1M stock	1	1 ml from 1M tock
		pH (with NaOH)	7.15
		Osmolarity (mOsm/L)	310

High Ca2+			
Compound	**M.W. (g/mol)**	**1X Concentration (mM)**	**For 1L (1X)**
NaCl	58.44	101.5	5.932 g
KCl	74.55	5	0.373 g
Proline	115.13	5	0.576 g
HEPES	238.30	10	2.383 g
Trehalose	378.33	5	3.78 g
Sucrose	342.30	32.5	11.125 g
CaCl2	1M stock	20	20 ml from 1M stock
MgCl2	1M stock	1	1 ml from 1M tock
		pH (with NaOH)	7.15
		Osmolarity (mOsm/L)	310

Isotonic (modified from *Drosophila* saline to maintain ionic balance across osmolarities)			
Compound	**M.W. (g/mol)**	**1X Concentration (mM)**	**For 1L (1X)**
NaCl	58.44	90	5.260 g
KCl	74.55	5	0.373 g
Proline	115.13	5	0.576 g
HEPES	238.30	10	2.383 g
Trehalose	378.33	5	3.78 g
Sucrose	342.30	92.5	31.663 g
CaCl2	1M stock	1.5	1.5 ml from 1M stock
MgCl2	1M stock	1	1 ml from 1M tock
		pH (with NaOH)	7.15
		Osmolarity (mOsm/L)	310

85% Hypoosmotic			
Compound	**M.W. (g/mol)**	**1X Concentration (mM)**	**For 1L (1X)**
NaCl	58.44	90	5.260 g
KCl	74.55	5	0.373 g
Proline	115.13	5	0.576 g
HEPES	238.30	10	2.383 g
Trehalose	378.33	5	3.78 g
Sucrose	342.30	46.5	15.917 g
CaCl2	1M stock	1.5	1.5 ml from 1M stock
MgCl2	1M stock	1	1 ml from 1M tock
		pH (with NaOH)	7.15
		Osmolarity (mOsm/L)	

70% Hypoosmotic			
Compound	**M.W. (g/mol)**	**1X Concentration (mM)**	**For 1L (1X)**
NaCl	58.44	90	5.260 g
KCl	74.55	5	0.373 g
Proline	115.13	5	0.576 g
HEPES	238.30	10	2.383 g
Trehalose	378.33	5	3.78 g
Sucrose	342.30	0	15.917 g
CaCl2	1M stock	1.5	1.5 ml from 1M stock
MgCl2	1M stock	1	1 ml from 1M tock
		pH (with NaOH)	7.15
		Osmolarity (mOsm/L)	